

PREPARED FOR SUBMISSION TO JHEP

NLO QCD corrections to off-shell $t\bar{t}W^\pm$ production at the LHC: Correlations and Asymmetries

Giuseppe Bevilacqua,^a Huan-Yu Bi,^b Heribertus Bayu Hartanto,^c Manfred Kraus,^d Jasmina Nasufi^b and Malgorzata Worek^b

^a*MTA-DE Particle Physics Research Group, University of Debrecen, H-4010 Debrecen, PBox 105, Hungary*

^b*Institute for Theoretical Particle Physics and Cosmology, RWTH Aachen University, D-52056 Aachen, Germany*

^c*Cavendish Laboratory, University of Cambridge, J.J. Thomson Avenue, Cambridge CB3 0HE, United Kingdom*

^d*Physics Department, Florida State University, Tallahassee, FL 32306-4350, USA*

E-mail: giuseppe.bevilacqua@science.unideb.hu,
bihy@physik.rwth-aachen.de, hbihartanto@hep.phy.cam.ac.uk,
mkraus@hep.fsu.edu, jasmina.nasufi@rwth-aachen.de,
worek@physik.rwth-aachen.de

ABSTRACT: Recent discrepancies between theoretical predictions and experimental data in multi-lepton plus b -jets analyses for the $t\bar{t}W^\pm$ process, as reported by the ATLAS collaboration, have indicated that more accurate theoretical predictions and high precision observables are needed to constrain numerous new physics scenarios in this channel. To this end we employ the NLO QCD computations with the full off-shell top quark effects included to provide theoretical predictions for the $\mathcal{R} = \sigma_{t\bar{t}W^+}/\sigma_{t\bar{t}W^-}$ cross section ratio at the LHC with $\sqrt{s} = 13$ TeV. Depending on the transverse momentum cut on the b -jet we obtain 1% – 2% theoretical precision on \mathcal{R} , which should help to shed some light on new physics effects that can reveal themselves only once sufficiently precise Standard Model theoretical predictions are available. Furthermore, triggered by these discrepancies we reexamine the top quark charge asymmetry and the charge asymmetries of the top quark decay products in the $t\bar{t}W^\pm$ production process. In the case of charge asymmetries, that are uniquely sensitive to the chiral nature of possible new physics in this channel, theoretical uncertainties below 15% have been obtained. Additionally, for both cases the impact of the top quark modelling is scrutinised by the explicit comparison with the predictions in the narrow-width approximation.

KEYWORDS: NLO Computations, QCD Phenomenology, Heavy Quark Physics

TTK-20-43, P3H-20-078, CAVENDISH-HEP-20/14

Contents

1	Introduction	1
2	Computational Framework and Input Parameters	4
3	Correlations between $t\bar{t}W^+$ and $t\bar{t}W^-$	5
4	Cross Section Ratios	11
5	Charge Asymmetries in $t\bar{t}W^\pm$ Production	13
6	Differential and cumulative asymmetry	19
7	Summary	23

1 Introduction

The Large Hadron Collider (LHC) with the Run II energy of $\sqrt{s} = 13$ TeV has opened up the possibility of studying various top quark production and decay mechanisms at larger mass scales than previously explored in any experiment. The $t\bar{t}$ pair production associated with the W^\pm gauge boson is among the most massive signatures that can be studied with high precision at the LHC. It is a key process to constrain top quark intrinsic properties, which might be modified in the presence of new physics. Moreover, the process can be used in the framework of the Standard Model Effective Field Theory (SMEFT), where the effects of potential new particles can be systematically included in terms of higher-dimensional operators. The latter are suppressed by a sufficiently large new physics energy scale Λ . The framework relies on the idea that new physics is too heavy to be directly produced and observed at the LHC, thus, only deviations from the Standard Model (SM) can be probed in various ATLAS and CMS top quark measurements. Compared with top quark pair production and single top quark production, the associated $t\bar{t}W^\pm$ process does not bring sensitivity to new operators, however, it helps to resolve blind directions in the SMEFT parameter space that occur in the current LHC fits. On top of that $t\bar{t}W^\pm$ can probe operators that are difficult to access in other channels. For example, since the W^\pm gauge boson is radiated from the initial state, $t\bar{t}W^\pm$ is sensitive to a subset of the possible four-quark operators only. In the SM, $t\bar{t}W^\pm$ is dominated by quark-antiquark interactions, while $t\bar{t}$ is dominated by the gg initial state. This means that relative to the SM contribution the four-quark operators would give sizeable effects in the $t\bar{t}W^\pm$ production process. Consequently, $t\bar{t}W^\pm$ production is often included in the global SMEFT analysis of LHC top quark measurements, see e.g. [1].

In addition, the $t\bar{t}W^\pm$ process play an important role in the studies of the top quark charge asymmetry denoted as A_c^t [2]. Also in this case the lack of the symmetric gg initial state and the emission of the W^\pm gauge boson from the initial states contribute to a substantially larger top quark charge asymmetry than that measured in the $t\bar{t}$ process. Furthermore, the asymmetry of the top quark decay products, i.e the charged lepton (A_c^ℓ) and the b -jet (A_c^b) are very large and already present at the LO due to the polarisation of the initial fermionic line by the W^\pm emission. These asymmetries are an interesting playground for various beyond the SM (BSM) theories, as A_c^t , A_c^ℓ and A_c^b are uniquely sensitive to the chiral nature of possible new physics that might directly affect such measurements.

Last but not least, $t\bar{t}W^\pm$ production is a background process in the multi-lepton final state with two same-sign leptons, accompanied by missing transverse momentum and b -jets [3–6]. Even though same-sign leptons are a relatively rare phenomenon in the SM, as they only appear in processes with a rather small cross section, they have been extensively exploited in various models of new physics. The same-sign lepton signature is present, among others, in models with supersymmetry, universal extra dimensions, top-quark partners and the extended Higgs boson sector [7–13]. Besides, same-sign leptons are considered a key feature in searches for heavy Majorana neutrinos as well as for $t\bar{t}$ and $t\bar{t}$ resonances [14, 15].

Finally, the $pp \rightarrow t\bar{t}W^\pm$ process is the main background in SM measurements involving final states with multiple leptons and b -jets. This is the case, for example, for the measurement of the associated production of the SM Higgs boson with top quarks [16]. The $pp \rightarrow t\bar{t}W^\pm$ process has also played a crucial role in the announcement of the strong evidence of the production of four top quarks, a measurement, which has been recently performed by the ATLAS Collaboration [17].

The direct measurement of $pp \rightarrow t\bar{t}W^\pm$ production in multi-lepton final states has already been carried out at $\sqrt{s} = 13$ TeV by the ATLAS and CMS collaborations [18–20]. In the recent measurement of $t\bar{t}H$ and $t\bar{t}W^\pm$ production in multi-lepton final states [16] the resulting $t\bar{t}W^\pm$ normalisation has been found to be higher than the theoretical prediction provided by the multipurpose Monte Carlo (MC) generators, which are currently employed by the ATLAS collaboration. Apart from the $t\bar{t}W^\pm$ normalisation, a tension in the modelling of the final state kinematics in the phase space regions dominated by $t\bar{t}W^\pm$ production, has been observed. From the experimental point of view such an accurate study of $pp \rightarrow t\bar{t}W^\pm$ production in the same-sign lepton final state has become feasible thanks to the increasing amount of data collected at the LHC with $\sqrt{s} = 13$ TeV. This increased integrated luminosity has significantly raised the need for more precise theoretical predictions. The latter should include higher order QCD corrections both to the production and decays of top quarks and W gauge bosons as well as incorporate $t\bar{t}$ spin correlations at the same level of accuracy.

The first calculations for the $pp \rightarrow t\bar{t}W^\pm$ process, that meet the mentioned conditions, have been carried out in the narrow-width approximation (NWA) within the MCFM framework [21]. The first full NLO QCD computations, which include complete top quark off-shell effects for the $pp \rightarrow t\bar{t}W^\pm$ process in the multi-lepton channel, have been recently presented in Ref. [22]. In these computations, obtained with the help of HELAC-NLO, off-shell top quarks have been described by Breit-Wigner propagators, furthermore, double-, single- as

well as non-resonant top-quark contributions along with all interference effects have been consistently incorporated at the matrix element level. Independent computations for $t\bar{t}W^+$ production have been obtained very recently within the MOCANLO+RECOLA framework [23]. They not only confirmed the results presented in Ref. [22] but also performed a comparison between the full results and those obtained with the help of the double-pole approximation. We also note that continuous efforts have been devoted to improve the theoretical modeling of hadronic observables at NLO through matching with parton shower and multi-jet merging [24–26] as well as by incorporating soft gluon resummation effects with the next-to-next-to-leading logarithmic (NNLL) accuracy [27–30].

In Ref. [22] results at NLO QCD accuracy have been presented in the form of fiducial integrated and differential cross sections for two selected renormalisation and factorisation scale choices (a fixed and a dynamical ones) and three different PDF sets. Detailed studies of the scale dependence of the NLO predictions have been carried out together with calculations of the PDF uncertainties. Furthermore, the impact of the top quark off-shell effects on the $pp \rightarrow t\bar{t}W^\pm$ cross section has been examined by an explicit comparison with the results in the NWA. In the current paper we will move away from the technical aspects of higher order calculations and the estimation of the residual theoretical uncertainties and go towards more phenomenological studies for the $pp \rightarrow t\bar{t}W^\pm$ process. Specifically, the purpose of this paper is twofold. First, we would like to provide a systematic analysis of the two processes $pp \rightarrow t\bar{t}W^+$ and $pp \rightarrow t\bar{t}W^-$ in the multi-lepton decay channel to extract the most accurate NLO QCD predictions for the $\mathcal{R} = \sigma_{t\bar{t}W^+}^{\text{NLO}}/\sigma_{t\bar{t}W^-}^{\text{NLO}}$ cross section ratio. Generally, the cross section ratios are more stable against radiative corrections than the absolute cross sections, assuming that the two processes are correlated. They have smaller theoretical uncertainties as various uncertainties tend to cancel in the cross section ratio. Consequently, such precise theoretical predictions have enhanced predictive power and should be used in indirect searches for new physics at the LHC. The second goal of the paper is to study separately the intrinsic properties of $t\bar{t}W^+$ and $t\bar{t}W^-$ production. More specifically, we shall use the state-of-the-art NLO QCD theoretical predictions for the $t\bar{t}W^\pm$ process to re-examine the top quark charge asymmetry and asymmetries of the top quark decay products both at the integrated and differential level. Likewise, in this case, the polarisation and asymmetry effects in the $pp \rightarrow t\bar{t}W^\pm$ production process can be employed to constrain new physics effects that might occur in this channel. Furthermore, for both the cross section ratio and the top quark (decay product) charge asymmetry, the impact of the modelling of top quark production and decays will be studied.

We note here, that the state-of-the-art theoretical predictions at NLO in QCD with the complete top quark off-shell effects included are also available for other processes at the LHC. Such effects, for example, have been incorporated for $pp \rightarrow t\bar{t}$ [31–34], $pp \rightarrow t\bar{t}j$ [35, 36], $pp \rightarrow t\bar{t}H$ [37], $pp \rightarrow t\bar{t}\gamma$ [38] and for $t\bar{t}Z(Z \rightarrow \nu_\ell \nu_\ell)$ [39]. Very recently they have also been incorporated for the $pp \rightarrow t\bar{t}b\bar{b}$ process [40].

The paper is organised as follows. In section 2 the HELAC-NLO computational framework and input parameters used in our studies are briefly described. In section 3 correlations between $t\bar{t}W^+$ and $t\bar{t}W^-$ are examined. The results for the cross section ratio $\mathcal{R} = \sigma_{t\bar{t}W^+}^{\text{NLO}}/\sigma_{t\bar{t}W^-}^{\text{NLO}}$ are provided in section 4. The integrated top quark charge asymmetry

as well as asymmetries of the top quark decay products are studied in section 5. Results for the differential and cumulative A_c^ℓ asymmetry are provided in section 6. Finally, in section 7 the results are summarised and our conclusions are provided.

2 Computational Framework and Input Parameters

All our results both for the full off-shell and NWA computations have been obtained with the help of the HELAC-NLO Monte Carlo framework [41]. The calculation was performed using HELAC-1LOOP [42, 43] for the virtual corrections and HELAC-DIPOLES [44, 45] for the real emission part. The integration over the phase space has been achieved with the help of KALEU [46]. In our studies we keep the Cabibbo-Kobayashi-Maskawa mixing matrix diagonal and neglect the Higgs boson contributions. Following recommendations of the PDF4LHC Working Group for the usage of PDFs suitable for applications at the LHC Run II [47] we employ the NNPDF3.0 PDF set [48]. In particular, we use NNPDF30-nlo-as-0118 with $\alpha_s(m_Z) = 0.118$ (NNPDF30-lo-as-0130 with $\alpha_s(m_Z) = 0.130$) at NLO (LO). The running of the strong coupling constant α_s with two-loop accuracy at NLO is provided by the LHAPDF interface [49]. The number of active flavours is set to $N_F = 5$. We employ the following SM input parameters

$$\begin{aligned} G_\mu &= 1.166378 \cdot 10^{-5} \text{ GeV}^{-2}, & m_t &= 172.5 \text{ GeV}, \\ m_W &= 80.385 \text{ GeV}, & \Gamma_W^{\text{NLO}} &= 2.09767 \text{ GeV}, \\ m_Z &= 91.1876 \text{ GeV}, & \Gamma_Z^{\text{NLO}} &= 2.50775 \text{ GeV}, \\ \Gamma_t^{\text{NLO}} &= 1.33247 \text{ GeV}, & \Gamma_{t,\text{NWA}}^{\text{NLO}} &= 1.35355 \text{ GeV}. \end{aligned} \tag{2.1}$$

For the W and Z gauge boson widths we use the NLO QCD values as calculated for $\mu_R = m_W$ and $\mu_R = m_Z$ respectively. All other partons, including bottom quarks, as well as leptons are treated as massless particles. The LO and NLO top quark widths are calculated according to Ref. [33]. The top quark width is treated as a fixed parameter throughout this work. Its value corresponds to a fixed scale $\mu_R = m_t$. The electromagnetic coupling α is calculated from the Fermi constant G_μ , i.e. in the G_μ -scheme, via

$$\alpha_{G_\mu} = \frac{\sqrt{2}}{\pi} G_\mu m_W^2 \sin^2 \theta_W, \tag{2.2}$$

where $\sin^2 \theta$ is defined according to

$$\sin^2 \theta = 1 - \frac{m_W^2}{m_Z^2}. \tag{2.3}$$

We use the kinematic-dependent factorisation and renormalisation scales $\mu_R = \mu_F = \mu_0$ with the central value $\mu_0 = H_T/3$ where H_T is the scalar sum of all transverse momenta in the event, including the missing transverse momentum. The latter is constructed from the three neutrinos ν_e , ν_e and ν_μ . The additional light jet, if resolved, is not included in the definition of H_T . In various comparisons we also use a fixed scale defined as $\mu_0 = m_t + m_W/2$. Jets are constructed out of all final-state partons with pseudo-rapidity $|\eta| < 5$

via the *anti*- k_T jet algorithm [50] with the separation parameter $R = 0.4$. We require exactly two b -jets and three charged leptons, two of which are same-sign leptons. All final states have to fulfil the following selection criteria that mimic very closely the ATLAS detector response [16]

$$\begin{aligned} p_{T,\ell} &> 25 \text{ GeV}, & p_{T,b} &> 25 \text{ GeV}, \\ |y_\ell| &< 2.5, & |y_b| &< 2.5, \\ \Delta R_{\ell\ell} &> 0.4, & \Delta R_{\ell b} &> 0.4, \end{aligned} \tag{2.4}$$

where ℓ stands for the charged lepton. We do not impose any restrictions on the kinematics of the additional light jet and the missing transverse momentum.

3 Correlations between $t\bar{t}W^+$ and $t\bar{t}W^-$

We start with the NLO QCD differential cross sections for $pp \rightarrow e^+\nu_e\mu^-\bar{\nu}_\mu e^+\nu_e b\bar{b} + X$ and $pp \rightarrow e^-\bar{\nu}_e\mu^+\nu_\mu e^-\bar{\nu}_e b\bar{b} + X$. They are obtained for the LHC Run II energy of $\sqrt{s} = 13$ TeV. For brevity, we will refer to these reactions as $pp \rightarrow t\bar{t}W^+$ and $pp \rightarrow t\bar{t}W^-$. We would like to understand similarities and potential differences between the two processes. We note that, at the leading order the production mechanism for $t\bar{t}W^+$ ($t\bar{t}W^-$) is via the scattering of up-type quark (anti-quark) and the corresponding down-type anti-quark (quark), i.e. $u\bar{d}$ and $c\bar{s}$ for $pp \rightarrow t\bar{t}W^+$ as well as $\bar{u}d$ and $\bar{c}s$ for $pp \rightarrow t\bar{t}W^-$. The quark-gluon initial state opens up only at the NLO in QCD. Similarities in the production mechanisms and final states suggest that the two processes are correlated. To show this we examine the common features in the kinematics of the final states. Since we are interested in the shape differences/similarities only and because the fiducial cross section for $pp \rightarrow t\bar{t}W^-$ is about a factor of two smaller than the one for the $pp \rightarrow t\bar{t}W^+$ process we concentrate on the normalised NLO QCD differential cross sections.

In the following the collection of leptonic observables will be examined. In the $pp \rightarrow t\bar{t}W^\pm$ process same-sign charged leptons $e^\pm e^\pm$ occur. In the case of final states with identical leptons the ordering in p_T has to be introduced to label the particles. To this end, we denote the first and the second hardest same-sign charged lepton as e_1^\pm and e_2^\pm respectively. In Figure 1 we present the NLO QCD differential cross sections for $pp \rightarrow t\bar{t}W^+$ and $pp \rightarrow t\bar{t}W^-$ as a function of the transverse momentum of e_1^\pm (p_{T,e_1}), the invariant mass of the $e_1^\pm e_2^\pm$ system (M_{e_1,e_2}) and the scalar sum of the transverse momenta of the charged leptons available in the given process (H_T^{lep}). The latter is defined as

$$H_T^{lep} = p_{T,\mu^\mp} + p_{T,e_1^\pm} + p_{T,e_2^\pm}. \tag{3.1}$$

Also shown in Figure 1 is the distance in the azimuthal angle rapidity plane between e_1^\pm and e_2^\pm ($\Delta R_{e_1,e_2}$). All differential cross section shown are, indeed, very similar.

In the next step we look at the b -jet kinematics. The two b -jets are ordered according to their p_T . The hardest (b_1) and the softest b -jet (b_2) kinematics are exhibited in Figure 2. We note here, however, that the charge identification of the b -jets is possible at the LHC, see e.g [51–54]. Thus, one can distinguish between b -jets initiated by b and \bar{b} . In this work,

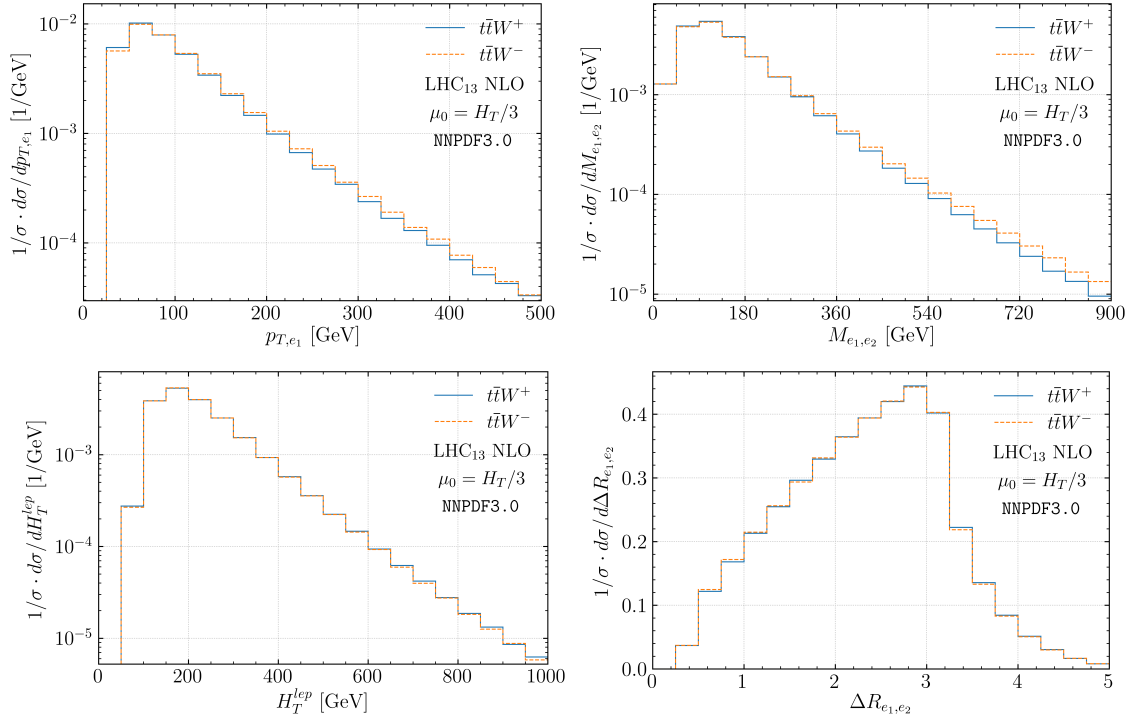


Figure 1. Comparison of the normalised NLO QCD differential cross sections for $pp \rightarrow t\bar{t}W^\pm$ in the multi-lepton final state at the LHC with $\sqrt{s} = 13$ TeV. The transverse momentum of the hardest same-sign lepton (p_{T,e_1}) and the invariant mass of the two same-sign leptons (M_{e_1,e_2}) are presented. Also given are the scalar sum of the transverse momenta of the leptons (H_T^{lep}) and the distance in the azimuthal angle rapidity plane between the two same-sign leptons ($\Delta R_{e_1,e_2}$). The NLO NNPDF3.0 PDF set is employed and $\mu_R = \mu_F = H_T/3$ is used.

however, we do not perform such b -jet identification. We depict the NLO QCD differential cross sections as a function of the transverse momentum of b_1 (p_{T,b_1}), the invariant mass of the two b -jet system (M_{b_1,b_2}) and the distance in the azimuthal angle rapidity plane between b_1 and b_2 ($\Delta R_{b_1,b_2}$). Also presented in Figure 2 is the scalar sum of the transverse momenta of all the visible final states, denoted as H_T^{vis} . The latter is given by

$$H_T^{vis} = p_{T,b_1} + p_{T,b_2} + p_{T,\mu^\mp} + p_{T,e_1^\pm} + p_{T,e_2^\pm}. \quad (3.2)$$

An interesting comment can be made here. Namely, that the b -jets are preferably produced in back-to-back configurations. Hereby, b -jets come more often from top quark decays rather than from the $g \rightarrow b\bar{b}$ splitting. The latter configuration, which is produced in the off-shell case where no top-quark resonances are presented, would manifest itself in the enhancement close to $\Delta R_{b_1,b_2} \approx 0.4$. In the case of b -jet kinematics and for the H_T^{vis} observable we can see similarities between $pp \rightarrow t\bar{t}W^+$ and $pp \rightarrow t\bar{t}W^-$.

To summarise this part, as anticipated both $t\bar{t}W^+$ and $t\bar{t}W^-$ production processes are highly correlated. This fact will be exploited when the theoretical uncertainties due to the scale dependence for the $t\bar{t}W^+$ and $t\bar{t}W^-$ cross section ratio will be estimated. For

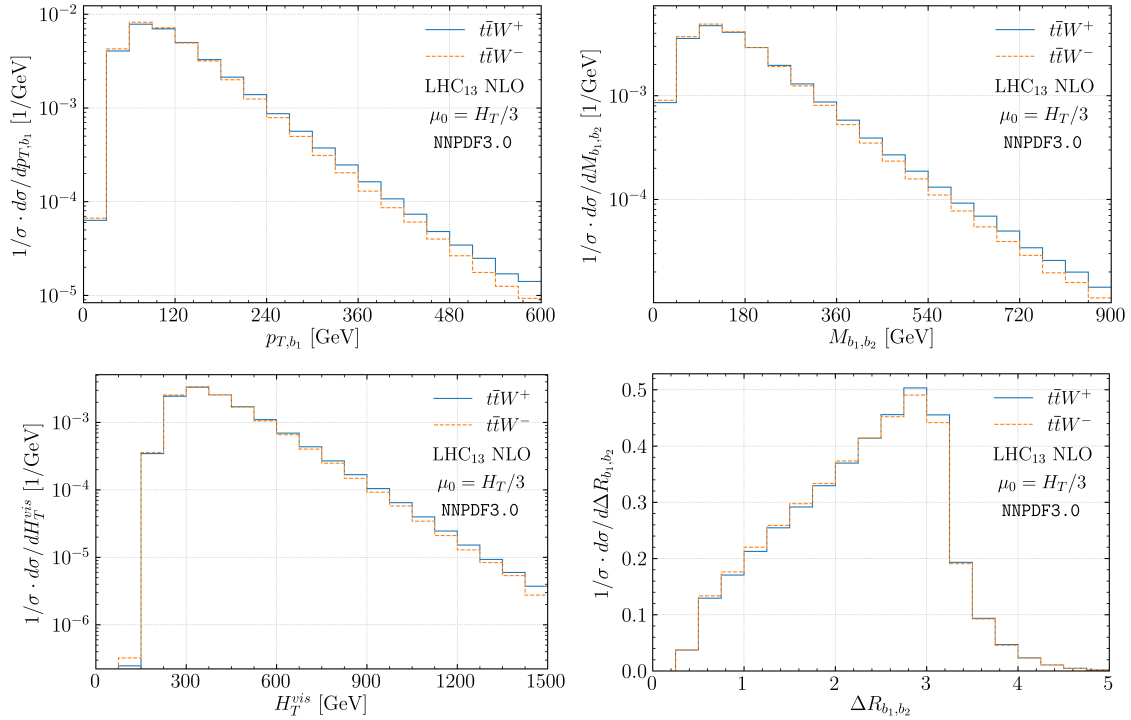


Figure 2. As in Figure 1 but for the transverse momentum of the hardest b -jet (p_{T,b_1}), the invariant mass of the two b -jets ($M_{b_1b_2}$), the scalar sum of the transverse momenta of the visible final states (H_T^{vis}) and the distance in the azimuthal angle rapidity plane between the two b -jets ($\Delta R_{b_1b_2}$).

both processes, our findings are not modified when the fixed scale choice $\mu_R = \mu_F = \mu_0 = m_t + m_W/2$ is used instead or when different PDF sets are employed.

So far, we have only used visual inspection to see whether two given one-dimensional normalised cross section distributions are similar or not. Even though this is an excellent place to start with, we would like to find a more quantitative approach to analyse the issue. In statistics literature several standard procedures exist for this task. Typically, the similarity of histograms is measured by a test statistic. The latter provides the quantitative expression of the distance between the two histograms that are compared. The smaller the distance the more similar are the compared histograms. There are several definitions of the test statistics in specialist literature on statistical methods. In the following we shall concentrate on the Kolmogorov-Smirnov test (KS-test) statistics. The purpose of the (two-sample) KS-test is to look for differences in the shape of two one-dimensional probability distributions. It is based on comparing two cumulative distribution functions (CDFs). The KS-test reports on the maximum difference between the two CDFs and calculates a p -value from that and the sample sizes. If the two tested histograms are indeed identical then they would have the same CDF. However, in reality two samples that are compared are randomly taken from their corresponding probability distributions. Therefore, even for the two truly identical histograms the corresponding CDFs will be slightly different. We can

use this fact to test the two distribution equality by comparing the KS-test statistic to 0. If the latter is significantly larger than 0 and close to 1, then we might conclude that the distributions are not equal and the two processes considered are not correlated. We continue with the differential cross section distribution for $pp \rightarrow t\bar{t}W^+$ and $pp \rightarrow t\bar{t}W^-$ as a function of the variable x , where x for example is $x = p_{T,e_1}, M_{e_1 e_2}$. When comparing both histograms, we use the same number of bins. We would like to verify the hypothesis that the two histograms are similar. To this end we calculate the KS-test statistics according to

$$\text{KS}_{\text{statistic}} = \sup_x |F_{n_1}^1(x) - F_{n_2}^2(x)|, \quad (3.3)$$

where $F_{n_1}^1$ and $F_{n_2}^2$ are the CDFs, n_1 and n_2 are the sizes of first and second sample respectively and \sup is the supremum function. We assume approximately 2000 events for $pp \rightarrow t\bar{t}W^+$ and about 1000 for $pp \rightarrow t\bar{t}W^-$, which correspond to the integrated LHC luminosity of $\mathcal{L} = 500 \text{ fb}^{-1}$ including a lepton-flavour factor of 8. After finding the maximum distance, we use the following condition

$$\sqrt{n} \text{KS}_{\text{statistic}} > \lambda(\alpha), \quad (3.4)$$

where

$$n = \frac{n_1 \cdot n_2}{n_1 + n_2}, \quad (3.5)$$

with $n_1 = 2000$, $n_2 = 1000$ and $\lambda(\alpha)$ is the threshold value that depends on the level of significance α . It can be found from the following condition

$$\mathcal{P}(\sqrt{n} \text{KS}_{\text{statistic}} > \lambda(\alpha)) = 1 - \mathcal{Q}_{\text{KS}}(\lambda(\alpha)) = \alpha, \quad (3.6)$$

where \mathcal{P} denotes probability and $\mathcal{Q}_{\text{KS}}(x)$ stands for the Kolmogorov-Smirnov distribution. We reject the hypothesis that the two distributions are similar if

$$\sqrt{n} \text{KS}_{\text{statistic}} > \lambda(\alpha), \quad (3.7)$$

and accept it when

$$\sqrt{n} \text{KS}_{\text{statistic}} \leq \lambda(\alpha). \quad (3.8)$$

We would normally start to question the hypothesis of the similarity of the histograms only if we find a difference larger than 2σ (the p -value smaller than 0.0455). If the difference is smaller than 2σ (the p -value larger than 0.0455) then we assume that the two tested distributions are indeed similar. Results that differ more than 3σ (the p -value smaller than 0.0027) can be directly translated into having enough evidence to reject the hypothesis, i.e. saying that there is a real difference between the two samples that are being studied. Note that the KS-test does not identify the source of the difference between histograms. It is a robust way of saying that there is a difference, however, the origin of such a difference must be identified by other means.

As the example in Figure 3 we present the distribution of the KS-test statistic for the following NLO QCD differential cross sections: p_{T,e_1} , M_{ee} , H_T^{lep} and ΔR_{ee} for $pp \rightarrow t\bar{t}W^+$ and $pp \rightarrow t\bar{t}W^-$. The total number of tries is set to $N_{\text{tries}} = 1000$. All KS-test statistic

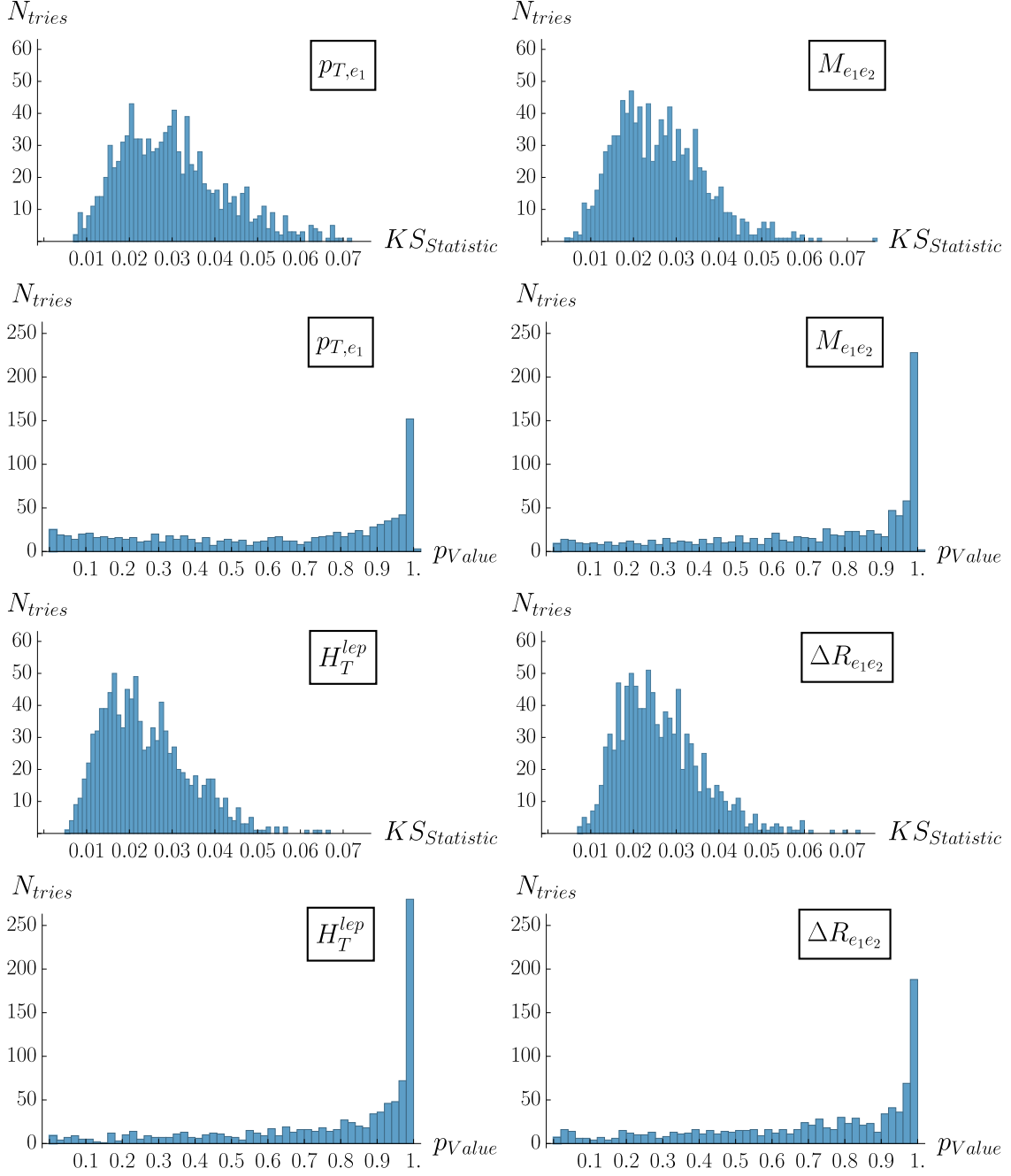


Figure 3. The distribution of the Kolmogorov-Smirnov test statistic (distance) for the null hypothesis of equality of the histogram shapes. NLO QCD differential cross section distributions for $pp \rightarrow t\bar{t}W^+$ and $pp \rightarrow t\bar{t}W^-$ in the multi-lepton final state are employed as a function of $p_{T,e1}$, M_{e1e2} , H_T^{lep} and ΔR_{e1e2} for the LHC with $\sqrt{s} = 13$ TeV. Also shown are the distributions of the corresponding p-values. The total number of N_{tries} is set to 1000.

values are distributed within the 0.01 – 0.07 range, i.e. very close to zero, which suggests that $pp \rightarrow t\bar{t}W^+$ and $pp \rightarrow t\bar{t}W^-$ are indeed correlated. Also shown in Figure 3 are the

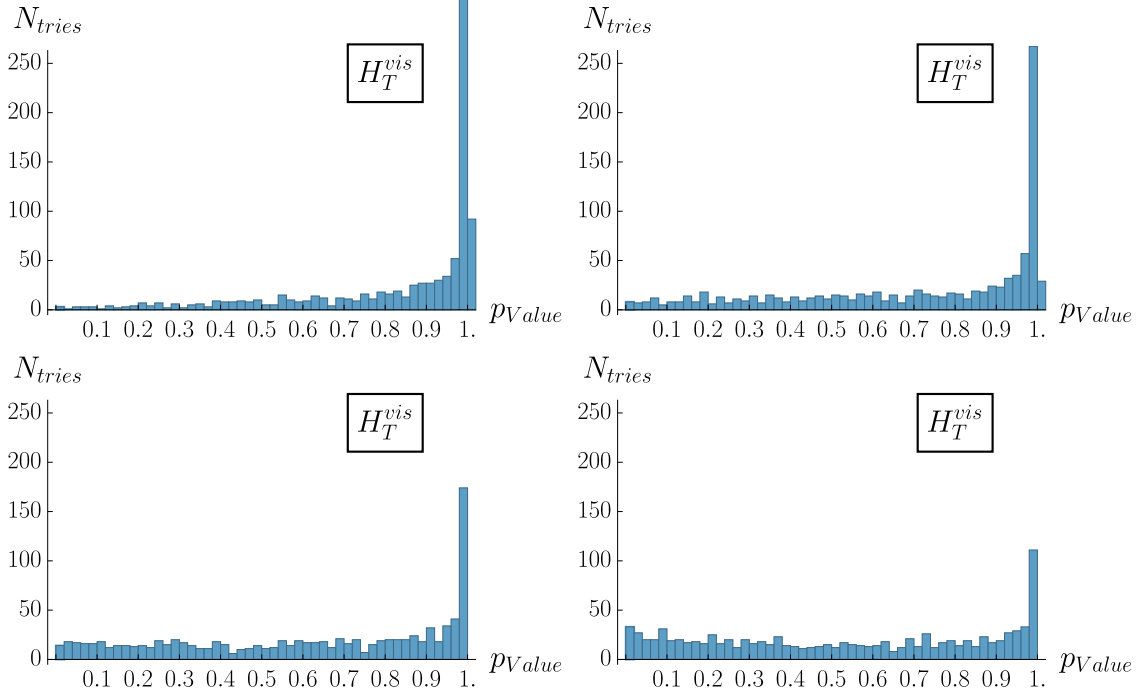


Figure 4. The distribution of p -values for the Kolmogorov-Smirnov test statistic for the NLO QCD differential cross section for $pp \rightarrow t\bar{t}W^+$ and $pp \rightarrow t\bar{t}W^-$ in the multi-lepton final state as a function of H_T^{vis} for the LHC with $\sqrt{s} = 13$ TeV. A different number of bins is assumed for each plot, however, the integrated luminosity is kept fixed. Specifically, we use the following four cases: 5 bins (upper left), 10 bins (upper right), 20 bins (lower left) and 40 bins (lower right). The total number of N_{tries} is set to 1000.

distributions of the corresponding p -values for the KS-test statistic. We can observe that the p -values are mostly distributed in the vicinity of 1, again supporting the hypothesis that $pp \rightarrow t\bar{t}W^+$ and $pp \rightarrow t\bar{t}W^-$ are highly correlated. We note here, that similar results have been obtained for the kinematics of the b -jet and for the H_T^{vis} observable.

We would like to stress at this point, that for the higher integrated luminosity or when the number of bins increases, the sensitivity of the KS-test increases as well. As an example we present in Figure 4 the distribution of p -values for the KS-test statistic for the H_T^{vis} observable for $pp \rightarrow t\bar{t}W^+$ and $pp \rightarrow t\bar{t}W^-$. We use four different values for the number of histogram bins, keeping the number of total events fixed for both processes. Specifically, we employ 5, 10, 20 and 40 bins respectively. We can observe that the percentage of N_{tries} with the p -value close to 1 is getting lower as the number of bins increases.

We summarise this part by noting, that there are many test statistics for the comparison of the shapes of two one-dimensional histograms. The most popular are: the Pearson- χ^2 test, the Anderson-Darling test or the Cramer-von-Mises test, see e.g. [55]. Each of these tests has its pros and cons and it is not possible to choose the one test that is the best for all applications. Overall, the more we know about what we really want to compare and test, the more reliable the test we can choose for our particular problem. We have examined

all the above-mentioned tests and have decided to use the Kolmogorov-Smirnov test of the equality. The two sample KS-test assumes continuous distributions. It is one of the most general nonparametric¹ tests for comparing two samples, as it is sensitive to differences in shape of the empirical cumulative distribution functions of the two samples. It is also the most robust test as it tests for any violation of the null hypothesis. However, it requires a relatively large number of data points in each bin. We further notice, that the KS-test is more sensitive to the regions near the peak of the tested distributions rather than to their tails. For the latter the Anderson-Darling test would do a better job. This observation is very useful in our case as for many dimensionful observables tails are usually plagued by larger statistical fluctuations and are, therefore, not really reliable for such comparisons.

4 Cross Section Ratios

Once we established that $pp \rightarrow t\bar{t}W^+$ and $t\bar{t}W^-$ are correlated we can look at their ratio with the goal of increasing the precision of NLO QCD predictions for both processes. The fact that the processes are correlated is exploited when estimating the theoretical error for the cross section ratio. Specifically, the theoretical error for the cross section ratio is estimated by calculating

$$\mathcal{R} = \frac{\sigma_{t\bar{t}W^+}^{\text{NLO}}(\mu_1)}{\sigma_{t\bar{t}W^-}^{\text{NLO}}(\mu_2)}, \quad (4.1)$$

with $\mu_1 = \mu_2 = \mu_0$ where $\mu_0 = m_t + m_W/2$ or $\mu_0 = H_T/3$. Furthermore, only the following combinations are considered

$$\left(\frac{\mu_1}{\mu_0}, \frac{\mu_2}{\mu_0}\right) = \{(2, 2), (0.5, 0.5)\}. \quad (4.2)$$

In Tables 1 and 2 we present integrated fiducial cross sections at NLO in QCD for $pp \rightarrow t\bar{t}W^+$ and $t\bar{t}W^-$ in the multi-lepton decay channel together with the theoretical uncertainties due to scale dependence. Also given is the \mathcal{R} cross section ratio. First we examine the stability of \mathcal{R} with respect to the $p_{T,b}$ cut. To this end, we show results for four different values of the $p_{T,b}$ cut. We observe very stable cross section ratio results both in terms of the central value and theoretical uncertainties. Furthermore, we notice that the scale choice does not play any role for such an inclusive observable. In the case of \mathcal{R} systematic uncertainties δ_{scale} and δ_{PDF} have been added in quadrature. We point out, however, that the PDF uncertainties, which for $pp \rightarrow t\bar{t}W^+$ and $pp \rightarrow t\bar{t}W^-$ are consistently at the 2% level, cancel out in the ratio to 0.2%. The final theoretical uncertainty is completely dominated by the scale dependence. The latter is at the 1% - 2% level. Such precise theoretical predictions have normally been obtained only once the NNLO QCD corrections are incorporated. Thus, \mathcal{R} at NLO in QCD represents a very precise observable to be measured at the LHC.

In the next step we examine the impact of the top quark production and decay modelling on the cross section ratio. To this end we present results for the full NWA and for the NWA_{LOdecay} case. The former comprises NLO QCD corrections to the production and

¹The nonparametric test does not assume that data points are sampled from the Gaussian distribution or any other defined distribution for that matter.

$\mu_0 = m_t + m_W/2$	$\sigma_{t\bar{t}W^+}^{\text{NLO}} \pm \delta_{\text{scale}} \pm \delta_{\text{PDF}}$	$\sigma_{t\bar{t}W^-}^{\text{NLO}} \pm \delta_{\text{scale}} \pm \delta_{\text{PDF}}$	$\sigma_{t\bar{t}W^+}^{\text{NLO}}/\sigma_{t\bar{t}W^-}^{\text{NLO}}$
NNPDF3.0	[ab]	[ab]	\mathcal{R}
$p_{T,b} > 25 \text{ GeV}$	$123.2^{+6.3(5\%)+2.1(2\%)}_{-8.7(7\%)-2.1(2\%)}$	$68.0^{+4.8(7\%)+1.2(2\%)}_{-5.5(8\%)-1.2(2\%)}$	$1.81 \pm 0.03 (2\%)$
$p_{T,b} > 30 \text{ GeV}$	$113.1^{+5.4(5\%)+1.9(2\%)}_{-7.8(7\%)-1.9(2\%)}$	$62.3^{+4.2(7\%)+1.1(2\%)}_{-4.9(8\%)-1.1(2\%)}$	$1.81 \pm 0.03 (2\%)$
$p_{T,b} > 35 \text{ GeV}$	$102.6^{+4.7(5\%)+1.7(2\%)}_{-6.8(7\%)-1.7(2\%)}$	$56.3^{+3.7(7\%)+1.0(2\%)}_{-4.4(8\%)-1.0(2\%)}$	$1.82 \pm 0.03 (2\%)$
$p_{T,b} > 40 \text{ GeV}$	$92.0^{+4.0(4\%)+1.6(2\%)}_{-6.1(7\%)-1.6(2\%)}$	$50.3^{+3.3(6\%)+0.9(2\%)}_{-3.9(8\%)-0.9(2\%)}$	$1.83 \pm 0.04 (2\%)$

Table 1. *NLO QCD integrated fiducial cross sections for $pp \rightarrow t\bar{t}W^\pm$ in the multi-lepton final state at the LHC with $\sqrt{s} = 13 \text{ TeV}$. Also shown are results for $\mathcal{R} = \sigma_{t\bar{t}W^+}^{\text{NLO}}/\sigma_{t\bar{t}W^-}^{\text{NLO}}$. Theoretical uncertainties as estimated from the scale variation and from the PDFs are listed as well. Four different values of the $p_{T,b}$ cut are used. The NNPDF3.0 PDF set is employed and $\mu_R = \mu_F = \mu_0$ where $\mu_0 = m_t + m_W/2$.*

to the subsequent top quark decays, the latter NLO QCD corrections to the production of $t\bar{t}W^\pm$ and LO top quark decays. Should we use the NLO QCD results in the full NWA for the $pp \rightarrow t\bar{t}W^\pm$ process our findings for $\mu_0 = m_t + m_W/2$ would be as follows

$$\mathcal{R} = \frac{\sigma_{t\bar{t}W^+}^{\text{NLO,NWA}}}{\sigma_{t\bar{t}W^-}^{\text{NLO,NWA}}} = 1.81 \pm 0.04 (2\%). \quad (4.3)$$

On the other hand for the dynamical scale choice $\mu_0 = H_T/3$ we would obtain

$$\mathcal{R} = \frac{\sigma_{t\bar{t}W^+}^{\text{NLO,NWA}}}{\sigma_{t\bar{t}W^-}^{\text{NLO,NWA}}} = 1.81 \pm 0.03 (2\%). \quad (4.4)$$

We can observe that the full NWA approach does not modify either the value or the size of the theoretical error for the integrated cross section ratio. The latter result is not surprising taking into account that the impact of the top quark off-shell effects on the integrated fiducial $t\bar{t}W^\pm$ cross section is negligible. Furthermore, theoretical uncertainties for the full NWA and full off-shell case are similar independently of the scale choice [22].

Finally, we have employed the $\text{NWA}_{\text{LOdecay}}$ case. For $\mu_0 = m_t + m_W/2$ we obtained

$$\mathcal{R} = \frac{\sigma_{t\bar{t}W^+}^{\text{NLO,NWA}_{\text{LOdecay}}}}{\sigma_{t\bar{t}W^-}^{\text{NLO,NWA}_{\text{LOdecay}}}} = 1.82 \pm 0.02 (1\%), \quad (4.5)$$

whereas for $\mu_0 = H_T/3$ we can report

$$\mathcal{R} = \frac{\sigma_{t\bar{t}W^+}^{\text{NLO,NWA}_{\text{LOdecay}}}}{\sigma_{t\bar{t}W^-}^{\text{NLO,NWA}_{\text{LOdecay}}}} = 1.81 \pm 0.02 (1\%). \quad (4.6)$$

$\mu_0 = H_T/3$ NNPDF3.0	$\sigma_{t\bar{t}W^+}^{\text{NLO}} \pm \delta_{\text{scale}} \pm \delta_{\text{PDF}}$ [ab]	$\sigma_{t\bar{t}W^-}^{\text{NLO}} \pm \delta_{\text{scale}} \pm \delta_{\text{PDF}}$ [ab]	$\sigma_{t\bar{t}W^+}^{\text{NLO}} / \sigma_{t\bar{t}W^-}^{\text{NLO}}$ \mathcal{R}
$p_{T,b} > 25 \text{ GeV}$	$124.4^{+4.3(3\%)+2.1(2\%)}_{-7.7(6\%)-2.1(2\%)}$	$68.6^{+3.5(5\%)+1.2(2\%)}_{-4.8(7\%)-1.2(2\%)}$	$1.81 \pm 0.02 (1\%)$
$p_{T,b} > 30 \text{ GeV}$	$113.9^{+3.5(3\%)+1.9(2\%)}_{-6.8(6\%)-1.9(2\%)}$	$62.7^{+3.0(5\%)+1.1(2\%)}_{-4.3(7\%)-1.1(2\%)}$	$1.82 \pm 0.03 (2\%)$
$p_{T,b} > 35 \text{ GeV}$	$103.1^{+3.1(3\%)+1.7(2\%)}_{-6.0(6\%)-1.7(2\%)}$	$56.5^{+2.6(5\%)+1.0(2\%)}_{-3.8(7\%)-1.0(2\%)}$	$1.82 \pm 0.02 (1\%)$
$p_{T,b} > 40 \text{ GeV}$	$92.3^{+2.8(3\%)+1.5(2\%)}_{-5.3(6\%)-1.5(2\%)}$	$50.4^{+2.3(5\%)+0.9(2\%)}_{-3.4(7\%)-0.9(2\%)}$	$1.83 \pm 0.03 (2\%)$

Table 2. As in Table 1 but for $\mu_0 = H_T/3$.

Even for this case the cross section ratios are very stable and rather insensitive to the details of the modelling of the top quark production and decays. Let us note here, that for the absolute $pp \rightarrow t\bar{t}W^\pm$ integrated cross sections the difference between the $\text{NWA}_{\text{LOdecay}}$ approach and the full off-shell one is at the level of 5%. In addition, theoretical uncertainties due to the scale dependence are higher in the former case, up to 11% – 13% [22]. Yet in the cross section ratio these differences cancel out making $\mathcal{R} = \sigma_{t\bar{t}W^+}^{\text{NLO}} / \sigma_{t\bar{t}W^-}^{\text{NLO}}$ very precise and an extremely interesting theoretical observable to be measured at the LHC.

To conclude this part, we note that for the cross section ratio at NLO in QCD the residual perturbative uncertainties are reduced to 1% – 2%. The theoretical uncertainties associated with the top quark modelling are negligible. This suggests that the $\mathcal{R} = \sigma_{t\bar{t}W^+}^{\text{NLO}} / \sigma_{t\bar{t}W^-}^{\text{NLO}}$ observable can be employed either for the precision SM measurements or to shed some light on possible new physics scenarios that might reveal themselves only once sufficiently precise theoretical predictions are available. In the case of the SM the \mathcal{R} observable, which is sensitive to the u/d valence content of the proton, can be used to provide valuable input for the up and down quark parton distribution functions of the proton at higher values of x (the momentum fraction of the parton). In the case of BSM physics the presence of two same-sign leptons in the final state, a rare phenomenon at the LHC, constitutes an optimal signature for many new physics models from supersymmetry, supergravity and Majorana neutrinos to models with the modified Higgs boson sector. Given the final accuracy of \mathcal{R} , it should be used to put more stringent constraints on the parameter space of these models.

5 Charge Asymmetries in $t\bar{t}W^\pm$ Production

The pp initial state at the LHC is expected to produce top quark and antiquark rapidity distributions in $t\bar{t}$ production that are symmetric about $y = 0$. However, since the quarks in the initial state can be from valence, while the antiquarks are from the sea, the larger average momentum-fraction of quarks leads to an excess of top quarks produced in the forward directions. The rapidity distribution of top quarks in the SM is therefore broader than that of the more centrally produced top antiquarks. This suggests that $\Delta|y| = |y_t| - |y_{\bar{t}}|$, which

is the difference between the absolute value of the top quark rapidity $|y_t|$ and the absolute value of the anti-top quark rapidity $|y_{\bar{t}}|$, is a suitable observable to measure the top quark charge asymmetry at the LHC. This asymmetry is nevertheless very small, see e.g. [56, 57]. For the $pp \rightarrow t\bar{t}W^\pm$ process the presence of the W^\pm gauge boson polarises the initial quark line and in turn the $t\bar{t}$ pair [2]. As a consequence the emerging top quark charge asymmetry is larger than that observed in $pp \rightarrow t\bar{t}$ production. Furthermore, the lepton and b -jet charge asymmetries are very large and already present at the leading order. In the following we calculate afresh the top quark charge asymmetry in the $t\bar{t}W^\pm$ process in the multi-lepton final state using the state-of-the-art NLO QCD calculations with the full top quark off-shell effects included. Additionally, the asymmetries for the top quark decay products, A_c^b and A_c^ℓ , will be examined. In this part of the paper, one of our main goals is to carefully assess the impact of the top quark modelling on A_c^t , A_c^b and A_c^ℓ . We start with asymmetries at the integrated level albeit in the fiducial regions of the phase space as defined in Section 2. For A_c^ℓ we will additionally calculate the differential and cumulative asymmetry with respect to the following observables: $p_T(\ell_t \ell_{\bar{t}})$, $|y(\ell_t \ell_{\bar{t}})|$ and $M(\ell_t \ell_{\bar{t}})$, where $\ell_t, \ell_{\bar{t}}$ stands for the charged leptons stemming from the top and anti-top quark decay respectively. For the two processes under consideration $pp \rightarrow e^+ \nu_e \mu^- \bar{\nu}_\mu e^+ \nu_e b\bar{b}$ and $pp \rightarrow e^- \bar{\nu}_e \mu^+ \nu_\mu e^- \bar{\nu}_e b\bar{b}$ the reconstruction of the (anti-)top quark momentum through its decay products is carried out. As we are dealing with identical leptons in the final state, however, we must employ an additional mechanism to properly assign the positron (electron) and the corresponding neutrino ν_e (anti-neutrino $\bar{\nu}_e$) to the correct top (anti-top) quark. In the case of $t\bar{t}W^+$ production we use the following four different resonance histories (a similar procedure is applied in the $t\bar{t}W^-$ case)

$$\begin{aligned}
t &\rightarrow e_1^+ \nu_{e,1} b & \text{and} & & \bar{t} &\rightarrow \mu^- \bar{\nu}_\mu \bar{b}, \\
t &\rightarrow e_1^+ \nu_{e,2} b & \text{and} & & \bar{t} &\rightarrow \mu^- \bar{\nu}_\mu \bar{b}, \\
t &\rightarrow e_2^+ \nu_{e,1} b & \text{and} & & \bar{t} &\rightarrow \mu^- \bar{\nu}_\mu \bar{b}, \\
t &\rightarrow e_2^+ \nu_{e,2} b & \text{and} & & \bar{t} &\rightarrow \mu^- \bar{\nu}_\mu \bar{b}.
\end{aligned} \tag{5.1}$$

These four resonant histories are not sufficient if NLO QCD calculations are considered. In the case of the subtracted real emission part we additionally take into account the extra light jet if resolved. Specifically, to closely mimic what is done on the experimental side only the light jet that passes all the cuts, that are also required for the two b -jets, is added to the resonance history. Thus, in such a case a total of twelve different resonant histories have to be considered. We compute for each history the following quantity, see Ref. [58]

$$\mathcal{Q} = |M_t - m_t| + |M_{\bar{t}} - m_t|, \tag{5.2}$$

where M_t and $M_{\bar{t}}$ are the (reconstructed) invariant masses of the top and anti-top quark respectively and $m_t = 172.5$ GeV. For each phase space point we pick the history that minimises the \mathcal{Q} value. In this way all the (anti-)top quark decay products are identified. They are employed in the definition of A_c^t , A_c^b and A_c^ℓ . To show how well such a reconstruction works in Figure 5 we display the reconstructed invariant mass of the top (anti-top) quark

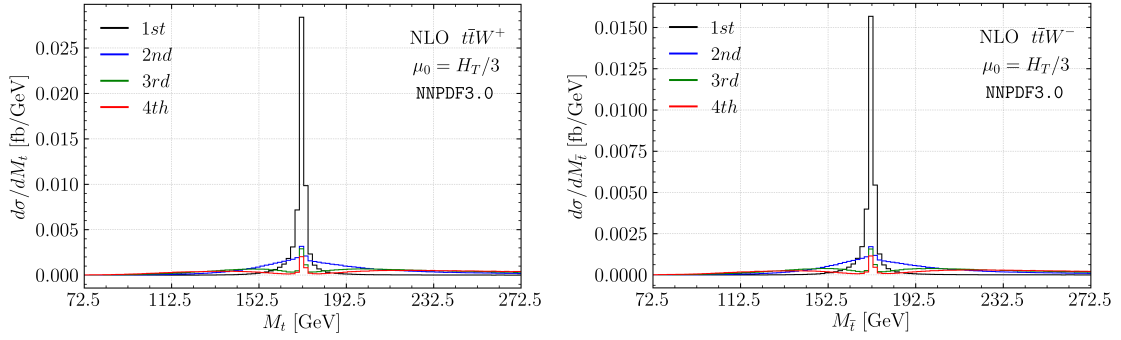


Figure 5. Reconstructed invariant mass of the top quark and anti-top quark at NLO in QCD for $pp \rightarrow t\bar{t}W^+$ and $pp \rightarrow t\bar{t}W^-$ in the multi-lepton final state. Results are given for the LHC with $\sqrt{s} = 13$ TeV. The NLO NNPDF3.0 PDF set is employed and $\mu_R = \mu_F = \mu_0$ where $\mu_0 = H_T/3$.

at NLO in QCD for the $pp \rightarrow t\bar{t}W^+$ ($pp \rightarrow t\bar{t}W^-$) process in the multi-lepton channel. Out of all twelve histories the four histories with the smallest Q value are shown. Clearly one can see that the reconstruction works very well.

Using the notation of Ref. [57, 59, 60] we define the top quark charge asymmetry as follows

$$A_c^t = \frac{\sigma_{\text{bin}}^+ - \sigma_{\text{bin}}^-}{\sigma_{\text{bin}}^+ + \sigma_{\text{bin}}^-}, \quad \sigma_{\text{bin}}^\pm = \int \theta(\pm \Delta|y|) \theta_{\text{bin}} d\sigma, \quad (5.3)$$

where $\Delta|y| = |y_t| - |y_{\bar{t}}|$ and $d\sigma$ is the differential fiducial $t\bar{t}W^\pm$ cross section calculated at NLO in QCD. The binning function θ_{bin} can take the values zero or one. Its purpose is to restrict to a given bin the kinematics of the $t\bar{t}W^\pm$ process in one of the kinematic variables that is considered. The integrated asymmetry is obtained by setting $\theta_{\text{bin}} = 1$. We note here that the charge-symmetric gg initial state, that is the dominant mechanism for $t\bar{t}$ production at the LHC, is not present for $t\bar{t}W^\pm$ production. Therefore, unlike for $pp \rightarrow t\bar{t}$, it will not contribute to the denominator of Eq. (5.3) to dilute the asymmetry. The LHC measurements for the top quark charge asymmetry in $pp \rightarrow t\bar{t}$ production have been carried out in terms of rapidity as well as pseudorapidity differences, see e.g. [61–66]. Even-though, the top quark charge asymmetry based on rapidity and pseudorapidity has the same features its value can differ quite substantially. Consequently, we shall provide results for A_c^t for both cases. In the case of the top quark decay products A_c^ℓ and A_c^b are based on $\Delta|y| = |y_{\ell_t}| - |y_{\ell_{\bar{t}}}|$ and $\Delta|y| = |y_b| - |y_{\bar{b}}|$ respectively.

The top quark charge asymmetry can be visualised by superimposing the rapidity (or the pseudo-rapidity) of t and \bar{t} for the $t\bar{t}W^+$ process. The same can be done separately for $t\bar{t}W^-$. Similarly, we can plot together the top and anti-top quark decay products, b and \bar{b} as well as ℓ_t and $\ell_{\bar{t}}$. In Figure 6 we present such a comparison at the NLO QCD level for the $t\bar{t}W^\pm$ process. We can observe that all spectra are symmetric about $y = 0$ ($\eta = 0$), as it should be, and that the anti-top quark is more central with respect to the top quark. The same is visible for the b -jet. This can be directly translated into the positive value of A_c^t and A_c^b . The situation is reversed for the charged leptons. In the later case the charged

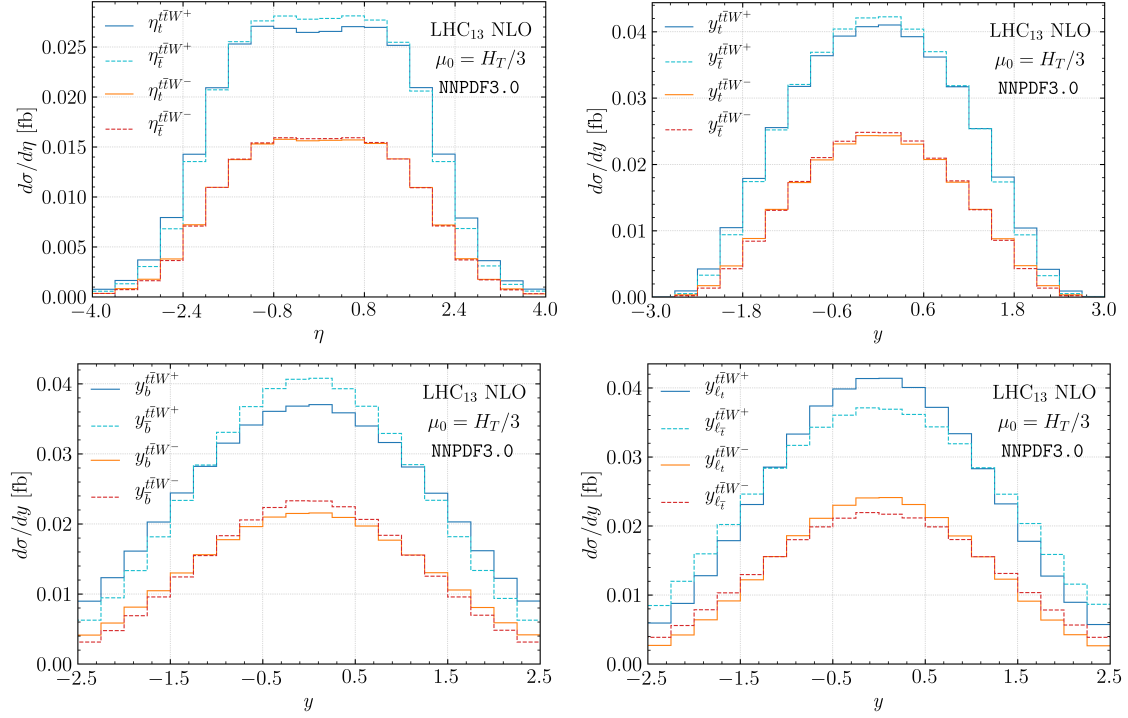


Figure 6. Comparison of the rapidity and pseudo-rapidity distributions of the t and \bar{t} quarks at the NLO QCD level for $pp \rightarrow t\bar{t}W^+$ and $pp \rightarrow t\bar{t}W^-$ in the multi-lepton final state. Also shown are rapidity distributions of the charged leptons and b -jets from t and \bar{t} decays. Results are given for the LHC with $\sqrt{s} = 13$ TeV. The NLO NNPDF3.0 PDF set is employed and $\mu_R = \mu_F = \mu_0$ where $\mu_0 = H_T/3$ is used.

lepton from the top quark decay is more central, which will manifest itself in the negative value of A_c^ℓ .

In Table 3 we present our findings for A_c^t , A_c^ℓ and A_c^b at NLO QCD for $t\bar{t}W^+$ production in the multi-lepton channel at the LHC with $\sqrt{s} = 13$ TeV. Results are given for the fixed scale choice $\mu_R = \mu_F = m_t + m_W/2$. The top quark charge asymmetry calculated in terms of rapidities (pseudo-rapidities) is denoted as $A_{c,y}^t$ ($A_{c,\eta}^t$). We present the results with the full off-shell effects included as well as for the full NWA and for the $\text{NWA}_{\text{LOdecay}}$ case. For all three approaches theoretical uncertainties due to the scale dependence are also given. They are estimated by varying the renormalisation and factorization scales in α_s and PDFs up and down by a factor 2 around the central scale of the process μ_0 . We show theoretical predictions for the unexpanded and expanded version of the asymmetry. The expanded version of A_c^i at NLO in QCD, where i stands for $i = t, \ell, b$, is defined as

$$A_{c,exp}^i = \frac{\sigma_{\text{LO}}^-}{\sigma_{\text{LO}}^+} \left(1 + \frac{\delta\sigma_{\text{NLO}}^-}{\sigma_{\text{LO}}^-} - \frac{\delta\sigma_{\text{NLO}}^+}{\sigma_{\text{LO}}^+} \right). \quad (5.4)$$

where σ^\pm stands for $\sigma^\pm = \sigma_{\text{bin}}^+ \pm \sigma_{\text{bin}}^-$ and $\delta\sigma_{\text{NLO}}^\pm$ are the NLO contributions to the fiducial cross section. Furthermore, σ_{LO}^\pm are evaluated with NLO input parameters. In the case of

$t\bar{t}W^+$ $\mu_0 = m_t + m_W/2$	OFF-SHELL	FULL NWA	NWA _{LOdecay}
$A_{c,y}^t$ [%]	$2.09(8)^{+1.06(51\%)}_{-0.70(33\%)}$	$1.68(4)^{+1.00(60\%)}_{-0.67(40\%)}$	$0.86(3)^{+0.66(77\%)}_{-0.43(50\%)}$
$A_{c,exp,y}^t$ [%]	$2.62(10)^{+0.39(15\%)}_{-0.34(13\%)}$	$2.19(4)^{+0.38(17\%)}_{-0.34(16\%)}$	$1.94(5)^{+0.46(24\%)}_{-0.32(16\%)}$
$A_{c,\eta}^t$ [%]	$3.10(8)^{+1.21(39\%)}_{-0.80(26\%)}$	$2.58(4)^{+1.31(51\%)}_{-0.75(29\%)}$	$1.16(4)^{+0.71(61\%)}_{-0.44(38\%)}$
$A_{c,exp,\eta}^t$ [%]	$3.70(10)^{+0.46(12\%)}_{-0.40(11\%)}$	$3.18(5)^{+0.56(18\%)}_{-0.34(11\%)}$	$2.25(5)^{+0.51(23\%)}_{-0.32(14\%)}$
$A_{c,y}^b$ [%]	$6.46(8)^{+0.05(0.8\%)}_{-0.05(0.8\%)}$	$6.18(4)^{+0.13(2.1\%)}_{-0.05(0.8\%)}$	$5.99(3)^{+0.10(1.7\%)}_{-0.01(0.2\%)}$
$A_{c,exp,y}^b$ [%]	$6.56(10)^{+0.02(0.3\%)}_{-0.07(1.1\%)}$	$6.28(4)^{+0.03(0.5\%)}_{-0.01(0.1\%)}$	$6.21(5)^{+0.06(1.0\%)}_{-0.01(0.2\%)}$
$A_{c,y}^\ell$ [%]	$-7.90(10)^{+2.15(27\%)}_{-1.39(17\%)}$	$-8.43(4)^{+2.10(25\%)}_{-1.37(16\%)}$	$-10.11(3)^{+1.36(13\%)}_{-0.95(9.4\%)}$
$A_{c,exp,y}^\ell$ [%]	$-7.00(12)^{+1.00(14\%)}_{-0.80(11\%)}$	$-7.52(4)^{+0.95(13\%)}_{-0.78(10\%)}$	$-8.23(5)^{+1.01(12\%)}_{-0.79(9.6\%)}$

Table 3. Unexpanded and expanded A_c^t , A_c^ℓ and A_c^b asymmetries at NLO in QCD for $pp \rightarrow t\bar{t}W^+$ in multi-lepton channel at the LHC with $\sqrt{s} = 13$ TeV. Various approaches for the modelling of the top quark production and decays are considered: the full off-shell case, the full NWA and the NWA_{LOdecay} case. Also given are Monte Carlo (in parenthesis) integration and theoretical errors. The NNPDF3.0 PDF set is employed and $\mu_R = \mu_F = \mu_0$ where $\mu_0 = m_t + m_W/2$.

large differences between the LO and NLO asymmetries, which is true for the $pp \rightarrow t\bar{t}W^\pm$ process, it is necessary to expand A_c^i to first order in α_s as the ratio in Eq. (5.3) generates contributions of $\mathcal{O}(\alpha_s^2)$ and higher, which are affected by the unknown NNLO contributions. Furthermore, in Table 3 we include in parenthesis the Monte Carlo (MC) integration errors to show that the latter are smaller than or at least similar in size to the theoretical errors from the scale dependence. Since the PDF dependence of the asymmetry is very small (at the per-mill level) we do not quote the PDF errors in our predictions.

In the following we analyse our findings that are presented in Table 3. We can first notice that the difference between the expanded and unexpanded asymmetries is rather moderate for the full off-shell and the full NWA case. We observe differences up to 25% – 30%. For the NWA_{LOdecay} approach, on the other hand, they are much larger, even above 100%. Secondly, theoretical uncertainties due to the scale dependence are substantially reduced for the expanded version of the asymmetries. In the case of the off-shell predictions, for example, we obtained 51%, 39% and 27% uncertainties for $A_{c,y}^t$, $A_{c,\eta}^t$ and $A_{c,y}^\ell$ respectively. Once the expansion is introduced 15%, 12%, 14% uncertainties are estimated instead. For the $A_{c,y}^b$ asymmetry no reduction is observed. Similar conclusions are obtained for the two other approaches. The two definitions, with unexpanded NLO asymmetry and with a consistent expansion in α_s , give reasonably consistent results for the central scale, especially

$t\bar{t}W^+$ $\mu_0 = H_T/3$	OFF-SHELL	FULL NWA	NWA _{LOdecay}
$A_{c,y}^t$ [%]	$2.36(8)^{+1.19(50\%)}_{-0.77(33\%)}$	$1.93(5)^{+1.23(64\%)}_{-0.72(37\%)}$	$1.11(3)^{+0.55(49\%)}_{-0.53(48\%)}$
$A_{c,exp,y}^t$ [%]	$2.66(10)^{+0.38(14\%)}_{-0.34(13\%)}$	$2.20(5)^{+0.45(20\%)}_{-0.31(14\%)}$	$2.08(5)^{+0.24(11\%)}_{-0.40(19\%)}$
$A_{c,\eta}^t$ [%]	$3.46(9)^{+1.41(41\%)}_{-0.90(26\%)}$	$3.02(5)^{+1.44(48\%)}_{-0.93(31\%)}$	$1.42(4)^{+0.59(41\%)}_{-0.56(39\%)}$
$A_{c,exp,\eta}^t$ [%]	$3.81(10)^{+0.46(12\%)}_{-0.40(10\%)}$	$3.36(5)^{+0.48(14\%)}_{-0.43(13\%)}$	$2.42(5)^{+0.27(11\%)}_{-0.44(18\%)}$
$A_{c,y}^b$ [%]	$6.48(9)^{+0.04(0.6\%)}_{-0.05(0.8\%)}$	$6.16(4)^{+0.07(1.1\%)}_{-0.01(0.2\%)}$	$6.05(3)^{+0.02(0.3\%)}_{-0.01(0.2\%)}$
$A_{c,exp,y}^b$ [%]	$6.53(10)^{+0.03(0.4\%)}_{-0.08(1.2\%)}$	$6.21(5)^{+0.09(1.4\%)}_{-0.05(0.8\%)}$	$6.23(5)^{+0.02(0.3\%)}_{-0.04(0.6\%)}$
$A_{c,y}^\ell$ [%]	$-7.46(11)^{+2.46(33\%)}_{-1.55(21\%)}$	$-7.94(4)^{+2.45(31\%)}_{-1.54(19\%)}$	$-9.81(4)^{+1.46(15\%)}_{-1.03(10\%)}$
$A_{c,exp,y}^\ell$ [%]	$-6.93(13)^{+1.01(14\%)}_{-0.81(12\%)}$	$-7.43(5)^{+0.99(13\%)}_{-0.79(11\%)}$	$-8.14(5)^{+1.00(12\%)}_{-0.81(10\%)}$

Table 4. As in Table 3 but for $\mu_0 = H_T/3$.

in the case of the full off-shell and NWA results. However, for the theoretical uncertainties large differences are observed in all three cases. Similar effects have been noticed for $A_{c,y}^t$ and $A_{c,exp,y}^t$ in the $pp \rightarrow t\bar{t}$ process at the LHC [57]. Once the next-to-next-to-leading order QCD corrections have been incorporated the difference between the expanded and unexpanded predictions has been reduced both for the central value and for the theoretical error underling the reliable theoretical control over these predictions. However, more important is the fact that the inclusion of the NNLO QCD corrections for $t\bar{t}$ has shown that theoretical uncertainties for the $A_{c,exp,y}^t$ observable are not underestimated at the NLO QCD level. Based on this argument and in the absence of NNLO QCD predictions for $pp \rightarrow t\bar{t}W^\pm$ process we can conclude that our expanded asymmetry results might be safely employed in the comparisons with the LHC experimental data. We can also note that the results for the top quark charge asymmetry based on the rapidity differences differ by almost 50% from those calculated in terms of pseudo-rapidity differences. Only in the case of NWA_{LOdecay} is the difference smaller, i.e. of the order of 15% – 35%. Finally, we compare the full off-shell case with the full NWA for the expanded asymmetries. For $A_{c,exp,y}^t$, $A_{c,exp,\eta}^t$ and $A_{c,exp,y}^\ell$ differences between central values are well below 1σ when compared with the respective theory uncertainties. This suggests that $A_{c,y}^t$, $A_{c,\eta}^t$ and $A_{c,y}^\ell$ are rather inclusive observables. For $A_{c,exp,y}^b$, however, for which theoretical uncertainties of the order of 1% are estimated, we obtained a substantial 3.7σ difference. This points to the conclusion that once the theoretical uncertainties are sufficiently reduced, the sensitivity of the asymmetries to the top quark production and decay modelling will increase. For now, however, the full NWA description is sufficient to describe (at least) $A_{c,exp,y}^t$, $A_{c,exp,\eta}^t$ and $A_{c,exp,y}^\ell$. In the next

step the $\text{NWA}_{\text{LOdecay}}$ case is compared to the full off-shell case. The discrepancies between central values of the asymmetries increased for $A_{c,exp,y}^t$, $A_{c,exp,\eta}^t$ and $A_{c,exp,y}^\ell$, in some cases even up to 2σ , while it remained almost the same for $A_{c,exp,y}^b$ (3.8σ). We can conclude that in the case of the top quark charge asymmetry and the asymmetries of the top quark decay products the NLO QCD corrections to the top quark decays play a crucial role. Overall, the inclusion of the complete off-shell effects for the $pp \rightarrow t\bar{t}W^+$ process increases the central values of the asymmetries while at the same time the theoretical errors are kept almost unchanged.

Our conclusions are not changed when the dynamical scale choice, $\mu_0 = H_T/3$, is employed instead. Results for $A_{c,y}^t$, $A_{c,\eta}^t$, $A_{c,y}^\ell$ and $A_{c,y}^b$ at NLO in QCD with $\mu_0 = H_T/3$ are shown in Table 4. When comparing to the theoretical predictions for $\mu_0 = m_t + m_W/2$ we can notice an overall agreement, within $0.1\sigma - 0.7\sigma$, between all central values of the asymmetries. In addition, similar theoretical uncertainties due to the scale dependence are estimated for both scale choices.

Our state-of-the art results for the top quark charge asymmetry and for the charge asymmetries of the top quark decay products are summarised in Table 5 and Table 6. In both cases we provide the NLO QCD results for the expanded version of A_c^t , A_c^ℓ and A_c^b . They are calculated from the theoretical predictions, which include the full top quark off-shell effects. We present results for $pp \rightarrow t\bar{t}W^+$ and $pp \rightarrow t\bar{t}W^-$ in the multi-lepton channel at the LHC with $\sqrt{s} = 13$ TeV. We additionally present the combined results for the $pp \rightarrow t\bar{t}W^\pm$ process. Also in this case the results for the top quark charge asymmetry are given in terms of rapidities, $\Delta|y| = |y_t| - |y_{\bar{t}}|$, and pseudorapidities, $\Delta|\eta| = |\eta_t| - |\eta_{\bar{t}}|$. A comment on the difference in size of asymmetries for $pp \rightarrow t\bar{t}W^+$ and $pp \rightarrow t\bar{t}W^-$ is in order. The asymmetries are larger for $pp \rightarrow t\bar{t}W^+$ than for $pp \rightarrow t\bar{t}W^-$. However, otherwise they behave similarly. As pointed out in Ref. [2] this can be understood by applying an argument based on PDFs. At the LO the $t\bar{t}W^+$ process is produced predominantly via $u\bar{d}$ whereas for $t\bar{t}W^-$ the $\bar{u}d$ subprocess is the most relevant one. The longitudinal momenta of the initial partons are on average $p_u > p_d > p_{\bar{u}} \approx p_{\bar{d}}$. In both cases the momentum of the top and anti-top quarks is connected to the momentum of the q and \bar{q} respectively. The large longitudinal momentum transferred to the top quark from the initial u quark in the $t\bar{t}W^+$ case increases the corresponding $|y_t|$ value. Consequently, the charge asymmetry of the top quark is enhanced compared to the one calculated for $t\bar{t}W^-$. When analysing the combined results for $pp \rightarrow t\bar{t}W^\pm$ we can observe that the theoretical uncertainties due to the scale dependence reach up to 15%. The scale choice play no role here as for $\mu_0 = m_t + m_W/2$ and $\mu_0 = H_T/3$ similar results are obtained.

6 Differential and cumulative asymmetry

In this part of the paper we present predictions for differential A_c^ℓ asymmetry with respect to the following observables: transverse momentum of the two charged leptons, $p_T(\ell_t\ell_{\bar{t}})$, rapidity of the two charged leptons, $|y(\ell_t\ell_{\bar{t}})|$, and invariant mass of the two charged leptons, $M(\ell_t\ell_{\bar{t}})$, where $\ell_t\ell_{\bar{t}}$ originate from the $t\bar{t}$ pair. The differential results are given using the unexpanded definition from Eq. (5.3). We also present predictions for cumulative asymme-

$\mu_0 = m_t + m_W/2$	$t\bar{t}W^+$	$t\bar{t}W^-$	$t\bar{t}W^\pm$
$A_{c,exp,y}^t$ [%]	$2.62^{+0.39}_{-0.34}$ (15%)	$1.97^{+0.31}_{-0.25}$ (16%)	$2.40^{+0.37}_{-0.31}$ (15%)
$A_{c,exp,\eta}^t$ [%]	$3.70^{+0.46}_{-0.40}$ (12%)	$1.31^{+0.32}_{-0.25}$ (24%)	$2.87^{+0.41}_{-0.35}$ (14%)
$A_{c,exp,y}^b$ [%]	$6.56^{+0.02}_{-0.07}$ (0.3%)	$4.80^{+0.05}_{-0.05}$ (1.0%)	$5.93^{+0.03}_{-0.08}$ (0.5%)
$A_{c,exp,y}^\ell$ [%]	$-7.00^{+1.00}_{-0.80}$ (14%)	$-5.68^{+0.78}_{-0.61}$ (14%)	$-6.51^{+0.93}_{-0.74}$ (14%)

Table 5. Expanded A_c^t , A_c^ℓ and A_c^b at NLO in QCD for $pp \rightarrow t\bar{t}W^+$ and $pp \rightarrow t\bar{t}W^-$ in the multi-lepton channel at the LHC with $\sqrt{s} = 13$ TeV. Results are obtained with the full off-shell effects included. Also given are combined results for $pp \rightarrow t\bar{t}W^\pm$ and theoretical uncertainties. The NNPDF3.0 PDF set is employed and $\mu_R = \mu_F = \mu_0$ where $\mu_0 = m_t + m_W/2$.

$\mu_0 = H_T/3$	$t\bar{t}W^+$	$t\bar{t}W^-$	$t\bar{t}W^\pm$
$A_{c,exp,y}^t$ [%]	$2.66^{+0.38}_{-0.34}$ (14%)	$2.05^{+0.33}_{-0.27}$ (16%)	$2.45^{+0.37}_{-0.31}$ (15%)
$A_{c,exp,\eta}^t$ [%]	$3.81^{+0.46}_{-0.40}$ (12%)	$1.31^{+0.33}_{-0.26}$ (25%)	$2.94^{+0.42}_{-0.35}$ (14%)
$A_{c,exp,y}^b$ [%]	$6.53^{+0.03}_{-0.08}$ (0.4%)	$4.80^{+0.06}_{-0.11}$ (1.2%)	$5.91^{+0.04}_{-0.09}$ (0.7%)
$A_{c,exp,y}^\ell$ [%]	$-6.93^{+1.01}_{-0.81}$ (14%)	$-5.67^{+0.81}_{-0.63}$ (14%)	$-6.46^{+0.95}_{-0.75}$ (15%)

Table 6. As in Table 5 but for $\mu_0 = H_T/3$.

tries, that are closely related to the corresponding differential asymmetries. One can employ the same definition as in Eq. (5.3), however, this time for a given value of the kinematic variable for which we compute the asymmetry the bin ranges from zero to that value. Even though differential and cumulative asymmetries contain the same information, the latter one behaves better simply because it is more inclusive, i.e. the higher order corrections are distributed more uniformly over the whole kinematic range. In addition, the cumulative asymmetry should give the integrated one in the last bin assuming that the plotted range of the corresponding differential distribution covers the whole available phase space. In practice, we shall see that if the left-over phase space region is negligible the integrated asymmetry can be recovered very accurately. Let us note that differential asymmetries have been studied at the LHC for the $pp \rightarrow t\bar{t}$ production process by both experimental collaborations ATLAS and CMS, see e.g. [65, 67].

In Figure 7 the $p_T(\ell_t \ell_{\bar{t}})$ -dependent differential and cumulative A_c^ℓ asymmetry at NLO QCD for $pp \rightarrow t\bar{t}W^\pm$ in multi-lepton channel at the LHC with $\sqrt{s} = 13$ TeV is displayed. Various approaches for the modelling of the top quark production and decays are considered. Also given are theoretical uncertainties for the full off-shell case. For all approaches Monte

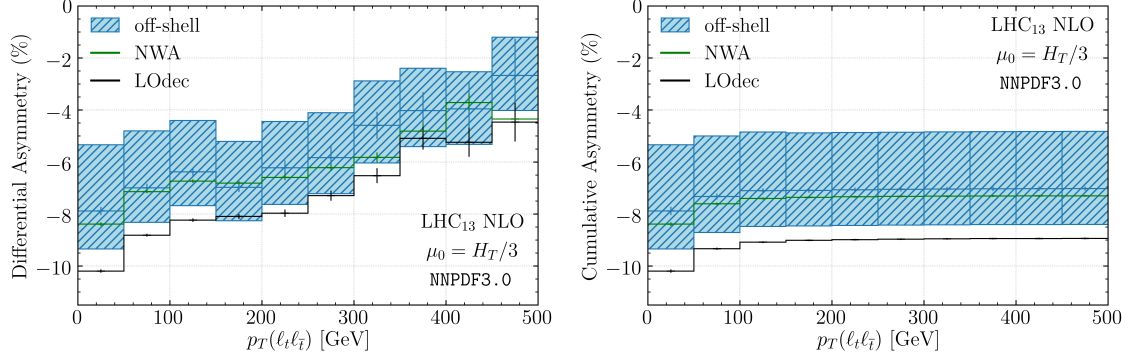


Figure 7. The $p_T(\ell_t \ell_{\bar{t}})$ -dependent differential (left panel) and cumulative (right panel) A_c^ℓ asymmetry at NLO QCD for $pp \rightarrow t\bar{t}W^\pm$ in the multi-lepton channel at the LHC with $\sqrt{s} = 13$ TeV. Various approaches for the modelling of the top quark production and decays are considered. Also given are theoretical uncertainties for the full off-shell case. For all approaches Monte Carlo errors are provided for both differential and cumulative asymmetries. The NNPDF3.0 PDF set is employed and $\mu_R = \mu_F = \mu_0$ where $\mu_0 = H_T/3$.

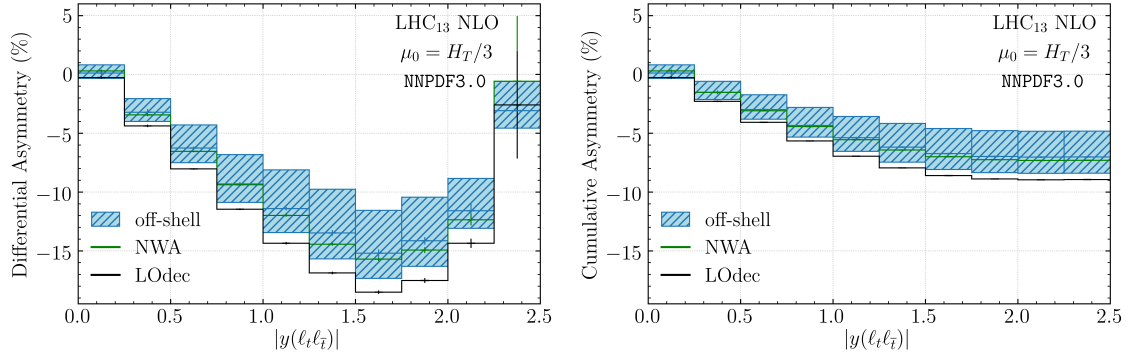


Figure 8. As in Figure 7 but for $|y(\ell_t \ell_{\bar{t}})|$.

Carlo integration errors are provided for both differential and cumulative asymmetries. For the $p_T(\ell_t \ell_{\bar{t}})$ -dependent differential asymmetry in all bins but the last the MC error is smaller than the theoretical one. In the last bin both uncertainties are comparable in size. The NNPDF3.0 PDF set is employed and μ_R as well as μ_F are set to the common value $\mu_R = \mu_F = \mu_0 = H_T/3$. For the differential A_c^ℓ asymmetry the difference between the full off-shell result and the full NWA case is in the 5% – 30% range depending on the bin, yet within theoretical uncertainties, that are of the order of 30%. We notice that this is not the case for the last bin where the top quark off-shell effects affect A_c^ℓ substantially. Specifically, they are above 60%. Also theoretical uncertainties increase in that bin and are of the order of 50%. The NWA_{LOdecay} case, on the other hand, is outside the scale dependence bands almost in the whole plotted range. The difference to the full off-shell approach is larger, even up to 70%. A similar effect is also visible for the cumulative asymmetry where a rather

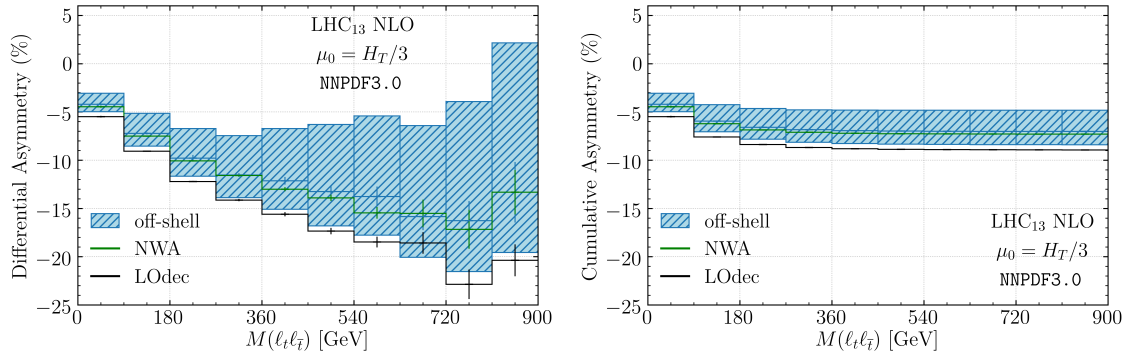


Figure 9. As in Figure 7 but for $M(\ell_t \ell_{\bar{t}})$.

constant 30% difference is noted for the $\text{NWA}_{\text{LOdecay}}$ case. Finally, we note that the last bin of the cumulative A_c^ℓ asymmetry gives $A_c^\ell = -7.02(8)$ for the complete off-shell case, $A_c^\ell = -7.30(4)$ for the full NWA and $A_c^\ell = -8.94(3)$ for the $\text{NWA}_{\text{LOdecay}}$ case, where in parentheses the MC error is displayed. All three results are indeed in perfect agreement within the MC errors with the corresponding results for the unexpanded leptonic charge asymmetry for the combined $pp \rightarrow t\bar{t}W^\pm$ process.

Similar observations can be made for the other two differential and cumulative A_c^ℓ asymmetries. The $|y(\ell_t \ell_{\bar{t}})|$ - and $M(\ell_t \ell_{\bar{t}})$ -dependent versions of A_c^ℓ are exhibited in Figure 8 and Figure 9 respectively. Since in each case the y axis is chosen to be the same for the differential and cumulative version of A_c^ℓ we can distinctly observe that the cumulative asymmetry behaves substantially better. Taking the differential $M(\ell_t \ell_{\bar{t}})$ -dependent version of A_c^ℓ as an example we observe large, of the order of 100%, theoretical uncertainties at the tails. On the other hand, the cumulative $M(\ell_t \ell_{\bar{t}})$ -dependent A_c^ℓ asymmetry has stable theoretical uncertainties of the order of 30% in the whole plotted range.

We summarise by noting, that several processes beyond the SM can alter A_c , see e.g. [2, 68–71], either with anomalous vector or axial-vector couplings or via interference with SM processes. Different models also predict different asymmetries as a function of the invariant mass and the transverse momentum, see e.g. [72]. Of course due to the much smaller cross section the $pp \rightarrow t\bar{t}W^\pm$ process will not replace the use of the asymmetries in $t\bar{t}$ production, however, it can provide a complementary tool as it is uniquely sensitive to the chiral nature of possible new physics that might manifest itself in this channel. This motivates our interest in the top quark charge asymmetry as well as the asymmetries of its decay products and their sensitivity to the top quark production and decay modelling. Furthermore, using our NLO QCD results with the full off-shell effects included, we are able to provide more precise theoretical predictions for A_c^t , A_c^ℓ and A_c^b in the $t\bar{t}W^\pm$ production process at the LHC with $\sqrt{s} = 13$ TeV. Finally, having at hand the full theory with no approximations included we are able to study the real size of theoretical uncertainties due to the scale dependence. In other words to verify whether they are under- or overestimated in the presence of various approximations.

7 Summary

In this paper we provided more accurate theoretical predictions for high precision observables, which should be used to constrain numerous new physics scenarios in the $t\bar{t}W^\pm$ channel. We considered the $t\bar{t}W^\pm$ production process in the multi-lepton decay channel for the LHC Run II energy of $\sqrt{s} = 13$ TeV for which discrepancies in the overall normalisation and in the modelling of the top quark decays have been recently reported by the ATLAS collaboration. Without the need of including terms beyond NLO in the perturbation expansion in α_s we obtained 1% – 2% theoretical uncertainties due to the scale dependence for this process by calculating the following cross section ratio $\mathcal{R} = \sigma_{t\bar{t}W^+}/\sigma_{t\bar{t}W^-}$. Such precision has been achieved as the two processes are indeed highly correlated. We proposed a rather simple method to examine the correlation between the two processes. Furthermore, fully realistic NLO QCD calculations have been employed in our studies for both $t\bar{t}W^+$ and $t\bar{t}W^-$. Specifically, we use $e^+\nu_e\mu^-\bar{\nu}_\mu e^+\nu_e b\bar{b}$ and $e^-\bar{\nu}_e\mu^+\nu_\mu e^-\bar{\nu}_e b\bar{b}$ matrix elements in our NLO QCD calculations. They include all resonant and non-resonant top quark and W gauge boson Feynman diagrams, their interference effects as well as off-shell effects of t and W . We examined the fixed and dynamical scale choice for μ_R and μ_F to assess their impact on the cross section ratio. We noticed that the scale choice does not play any role for such an inclusive observable. In the next step we examined the impact of the top quark production and decay modelling on the cross section ratio. We observed that the full NWA approach does not modify either the value or the size of the theoretical error for the integrated cross section ratio. Even for the simplified version of the NWA, i.e. for the $\text{NWA}_{\text{LOdecays}}$ case, no changes have been observed. Thus, the $\mathcal{R} = \sigma_{t\bar{t}W^+}/\sigma_{t\bar{t}W^-}$ observable is very stable and insensitive to the details of the modelling of the top quark decay chain. As such, it can be safely exploited at the LHC either for the precision SM measurements or in searches for BSM physics. Because the \mathcal{R} observable is sensitive to the u/d valence content of the proton it can be used, for example, to provide valuable input for the up and down quark parton distribution functions. In the case of new physics searches the presence of two same-sign leptons in the final state offers a very interesting signature, that has been highly scrutinised in many new physics models. The latter range from supersymmetry and supergravity to the more specific scenarios with the Majorana neutrinos and the modified Higgs boson sector. Given the final accuracy of \mathcal{R} and its insensitivity to the top quark modelling, the \mathcal{R} observable should be used at the LHC, for example to achieve more stringent constrain limits on the parameter space of these models.

In the second part of the paper we reexamined the top quark charge asymmetry and the charge asymmetries of the top quark decay products for the $t\bar{t}W^\pm$ process in the fiducial phase-space regions. Also in this case the state-of-the-art NLO QCD theoretical predictions were utilised. We presented predictions for the expanded and unexpanded asymmetries. As large differences have been observed only the expanded results should be used in practice. Furthermore, we have compared the full off-shell case with the results in the NWA. For $A_{c,exp,y}^t$, $A_{c,exp,\eta}^t$ and $A_{c,exp,y}^\ell$, for which theoretical uncertainties of the order of 15% have been estimated, we have observed differences below 1σ . This finding suggests a rather inclusive nature of these observables. One has to keep in mind, however, that the final

uncertainties on $A_{c,exp,y}^t$, $A_{c,exp,\eta}^t$ and $A_{c,exp,y}^\ell$ are rather moderate. For A_c^b , on the other hand, for which theoretical uncertainties are very small, i.e. of the order of 1%, a 4σ difference has been obtained. We can conclude that once theoretical uncertainties due to the scale dependence are sufficiently reduced, the sensitivity of the charge asymmetries to the top quark modelling might indeed increase. With the theoretical uncertainties at hand, however, the full NWA description is perfectly adequate. In the next step the $NWA_{LOdecay}$ case has been compared to the full off-shell one. In this case the discrepancies between central values of the asymmetries have increased even up to 2σ . The latter fact indicates that NLO QCD corrections to the top quark decays play a crucial role here. Overall, the inclusion of the complete description for the $pp \rightarrow t\bar{t}W^\pm$ process in the multi-lepton final state has increased the central values of the asymmetries keeping at the same time the theoretical errors unchanged. We reported on our state-of-the-art results for the top quark charge asymmetry and for the charge asymmetries of the top quark decay products separately for $pp \rightarrow t\bar{t}W^+$ and $pp \rightarrow t\bar{t}W^-$ as well as for the combined $pp \rightarrow t\bar{t}W^\pm$ process. The scale choice has played no role as for $\mu_0 = m_t + m_W/2$ and $\mu_0 = H_T/3$ similar results have been obtained for A_c^t , A_c^ℓ and A_c^b .

Furthermore, we presented predictions for the differential and cumulative A_c^ℓ asymmetry with respect to $p_T(\ell_t\ell_{\bar{t}})$, $|y(\ell_t\ell_{\bar{t}})|$ and $M(\ell_t\ell_{\bar{t}})$. The advantage of choosing A_c^ℓ lies in the fact that the measurements of the charged leptons are particularly precise at the LHC due to the excellent lepton energy resolution of the ATLAS and CMS detectors. We note here that for these studies the unexpanded version of A_c^ℓ has been examined. Depending on the bin the differences between the full off-shell results and the full NWA ones have been in the 5% – 30% range. However, this is well within theoretical uncertainties, that are of the order of 30%. On the other hand, large differences have been noticed for the $NWA_{LOdecay}$ case even up to 70%. Similarly for the cumulative asymmetry the $NWA_{LOdecay}$ curves are lying outside the uncertainty bands independently of the observable and the considered bin. We would like to add here that even though differential and cumulative asymmetries contain the same information, the latter behaves better simply because it is more inclusive. In other words, the higher order corrections are distributed more uniformly over the whole kinematic range.

Last but not least, several BSM physics scenarios can alter the top quark charge asymmetry. Thus, theoretical predictions for the A_c^t , A_c^ℓ and A_c^b quantities should be as accurate as possible. Using our NLO QCD results with the full off-shell effects included not only are we able to provide the state-of-the-art theoretical predictions for A_c^t , A_c^ℓ and A_c^b in the $t\bar{t}W^\pm$ production process but we could also carefully examine the real size of theoretical uncertainties due to the scale dependence.

Acknowledgments

This research of H.Y.B., J.N. and M.W. was supported by the Deutsche Forschungsgemeinschaft (DFG) under the following grants: 400140256 - GRK 2497: *The physics of the heaviest particles at the Large Hardon Collider* and 396021762 - TRR 257: *P3H - Particle Physics Phenomenology after the Higgs Discovery*.

Support by a grant of the Bundesministerium für Bildung und Forschung (BMBF) is additionally acknowledged.

The work of G.B. was supported by grant K 125105 of the National Research, Development and Innovation Office in Hungary.

H.B.H. has received funding from the European Research Council (ERC) under the European Union’s Horizon 2020 Research and Innovation Programme (grant agreement no. 683211 and 772099). Furthermore, the work of H.B.H has been partially supported by STFC consolidated HEP theory grant ST/T000694/1.

Simulations were performed with computing resources granted by RWTH Aachen University under project `rwth0414`.

References

- [1] I. Brivio, S. Bruggisser, F. Maltoni, R. Moutafis, T. Plehn, E. Vryonidou et al., *O new physics, where art thou? A global search in the top sector*, *JHEP* **02** (2020) 131 [[1910.03606](#)].
- [2] F. Maltoni, M. Mangano, I. Tsinikos and M. Zaro, *Top-quark charge asymmetry and polarization in $t\bar{t}W^\pm$ production at the LHC*, *Phys. Lett. B* **736** (2014) 252 [[1406.3262](#)].
- [3] ATLAS collaboration, *Search for supersymmetry at $\sqrt{s} = 13$ TeV in final states with jets and two same-sign leptons or three leptons with the ATLAS detector*, *Eur. Phys. J. C* **76** (2016) 259 [[1602.09058](#)].
- [4] CMS collaboration, *Search for new physics in same-sign dilepton events in proton–proton collisions at $\sqrt{s} = 13$ TeV*, *Eur. Phys. J. C* **76** (2016) 439 [[1605.03171](#)].
- [5] CMS collaboration, *Search for physics beyond the standard model in events with two leptons of same sign, missing transverse momentum, and jets in proton–proton collisions at $\sqrt{s} = 13$ TeV*, *Eur. Phys. J. C* **77** (2017) 578 [[1704.07323](#)].
- [6] ATLAS collaboration, *Search for supersymmetry in final states with two same-sign or three leptons and jets using 36 fb^{-1} of $\sqrt{s} = 13$ TeV pp collision data with the ATLAS detector*, *JHEP* **09** (2017) 084 [[1706.03731](#)].
- [7] R. Barnett, J. F. Gunion and H. E. Haber, *Discovering supersymmetry with like sign dileptons*, *Phys. Lett. B* **315** (1993) 349 [[hep-ph/9306204](#)].
- [8] M. Guchait and D. Roy, *Like sign dilepton signature for gluino production at CERN LHC including top quark and Higgs boson effects*, *Phys. Rev. D* **52** (1995) 133 [[hep-ph/9412329](#)].
- [9] H. Baer, C.-h. Chen, F. Paige and X. Tata, *Signals for minimal supergravity at the CERN large hadron collider. 2: Multi - lepton channels*, *Phys. Rev. D* **53** (1996) 6241 [[hep-ph/9512383](#)].
- [10] J. Maalampi and N. Romanenko, *Single production of doubly charged Higgs bosons at hadron colliders*, *Phys. Lett. B* **532** (2002) 202 [[hep-ph/0201196](#)].
- [11] H.-C. Cheng, K. T. Matchev and M. Schmaltz, *Bosonic supersymmetry? Getting fooled at the CERN LHC*, *Phys. Rev. D* **66** (2002) 056006 [[hep-ph/0205314](#)].
- [12] H. Dreiner, S. Grab, M. Kramer and M. Trenkel, *Supersymmetric NLO QCD corrections to resonant slepton production and signals at the Tevatron and the CERN LHC*, *Phys. Rev. D* **75** (2007) 035003 [[hep-ph/0611195](#)].

- [13] R. Contino and G. Servant, *Discovering the top partners at the LHC using same-sign dilepton final states*, *JHEP* **06** (2008) 026 [[0801.1679](#)].
- [14] J. Almeida, F.M.L., Y. do Amaral Coutinho, J. A. Martins Simoes, P. Queiroz Filho and C. Porto, *Same sign dileptons as a signature for heavy Majorana neutrinos in hadron hadron collisions*, *Phys. Lett. B* **400** (1997) 331 [[hep-ph/9703441](#)].
- [15] Y. Bai and Z. Han, *Top-antitop and Top-top Resonances in the Dilepton Channel at the CERN LHC*, *JHEP* **04** (2009) 056 [[0809.4487](#)].
- [16] ATLAS collaboration, *Analysis of $t\bar{t}H$ and $t\bar{t}W$ production in multilepton final states with the ATLAS detector*, *ATLAS-CONF-2019-045* (2019) .
- [17] ATLAS collaboration, *Evidence for $t\bar{t}t\bar{t}$ production in the multilepton final state in proton-proton collisions at $\sqrt{s}=13$ TeV with the ATLAS detector*, [2007.14858](#).
- [18] ATLAS collaboration, *Measurement of the $t\bar{t}Z$ and $t\bar{t}W$ production cross sections in multilepton final states using 3.2 fb^{-1} of pp collisions at $\sqrt{s} = 13$ TeV with the ATLAS detector*, *Eur. Phys. J. C* **77** (2017) 40 [[1609.01599](#)].
- [19] CMS collaboration, *Measurement of the cross section for top quark pair production in association with a W or Z boson in proton-proton collisions at $\sqrt{s} = 13$ TeV*, *JHEP* **08** (2018) 011 [[1711.02547](#)].
- [20] ATLAS collaboration, *Measurement of the $t\bar{t}Z$ and $t\bar{t}W$ cross sections in proton-proton collisions at $\sqrt{s} = 13$ TeV with the ATLAS detector*, *Phys. Rev. D* **99** (2019) 072009 [[1901.03584](#)].
- [21] J. M. Campbell and R. Ellis, *$t\bar{t}W^\pm$ production and decay at NLO*, *JHEP* **07** (2012) 052 [[1204.5678](#)].
- [22] G. Bevilacqua, H.-Y. Bi, H. B. Hartanto, M. Kraus and M. Worek, *The simplest of them all: $t\bar{t}W^\pm$ at NLO accuracy in QCD*, *JHEP* **08** (2020) 043 [[2005.09427](#)].
- [23] A. Denner and G. Pelliccioli, *NLO QCD corrections to off-shell $t\bar{t}W^+$ production at the LHC*, [2007.12089](#).
- [24] M. Garzelli, A. Kardos, C. Papadopoulos and Z. Trocsanyi, *$t\bar{t}W^\pm$ and $t\bar{t}Z$ Hadroproduction at NLO accuracy in QCD with Parton Shower and Hadronization effects*, *JHEP* **11** (2012) 056 [[1208.2665](#)].
- [25] R. Frederix and I. Tsinikos, *Subleading EW corrections and spin-correlation effects in $t\bar{t}W$ multi-lepton signatures*, *Eur. Phys. J. C* **80** (2020) 803 [[2004.09552](#)].
- [26] S. von Buddenbrock, R. Ruiz and B. Mellado, *Anatomy of inclusive $t\bar{t}W$ production at hadron colliders*, [2009.00032](#).
- [27] H. T. Li, C. S. Li and S. A. Li, *Renormalization group improved predictions for $t\bar{t}W^\pm$ production at hadron colliders*, *Phys. Rev. D* **90** (2014) 094009 [[1409.1460](#)].
- [28] A. Broggio, A. Ferroglia, G. Ossola and B. D. Pecjak, *Associated production of a top pair and a W boson at next-to-next-to-leading logarithmic accuracy*, *JHEP* **09** (2016) 089 [[1607.05303](#)].
- [29] A. Kulesza, L. Motyka, D. Schwartländer, T. Stebel and V. Theeuwes, *Associated production of a top quark pair with a heavy electroweak gauge boson at NLO+NNLL accuracy*, *Eur. Phys. J. C* **79** (2019) 249 [[1812.08622](#)].

- [30] A. Kulesza, L. Motyka, D. Schwartländer, T. Stebel and V. Theeuwes, *Associated top quark pair production with a heavy boson: differential cross sections at NLO+NNLL accuracy*, *Eur. Phys. J. C* **80** (2020) 428 [[2001.03031](#)].
- [31] A. Denner, S. Dittmaier, S. Kallweit and S. Pozzorini, *NLO QCD corrections to WWbb production at hadron colliders*, *Phys. Rev. Lett.* **106** (2011) 052001 [[1012.3975](#)].
- [32] G. Bevilacqua, M. Czakon, A. van Hameren, C. G. Papadopoulos and M. Worek, *Complete off-shell effects in top quark pair hadroproduction with leptonic decay at next-to-leading order*, *JHEP* **02** (2011) 083 [[1012.4230](#)].
- [33] A. Denner, S. Dittmaier, S. Kallweit and S. Pozzorini, *NLO QCD corrections to off-shell top-antitop production with leptonic decays at hadron colliders*, *JHEP* **10** (2012) 110 [[1207.5018](#)].
- [34] A. Denner and M. Pellen, *Off-shell production of top-antitop pairs in the lepton+jets channel at NLO QCD*, *JHEP* **02** (2018) 013 [[1711.10359](#)].
- [35] G. Bevilacqua, H. Hartanto, M. Kraus and M. Worek, *Top Quark Pair Production in Association with a Jet with Next-to-Leading-Order QCD Off-Shell Effects at the Large Hadron Collider*, *Phys. Rev. Lett.* **116** (2016) 052003 [[1509.09242](#)].
- [36] G. Bevilacqua, H. Hartanto, M. Kraus and M. Worek, *Off-shell Top Quarks with One Jet at the LHC: A comprehensive analysis at NLO QCD*, *JHEP* **11** (2016) 098 [[1609.01659](#)].
- [37] A. Denner and R. Feger, *NLO QCD corrections to off-shell top-antitop production with leptonic decays in association with a Higgs boson at the LHC*, *JHEP* **11** (2015) 209 [[1506.07448](#)].
- [38] G. Bevilacqua, H. Hartanto, M. Kraus, T. Weber and M. Worek, *Hard Photons in Hadroproduction of Top Quarks with Realistic Final States*, *JHEP* **10** (2018) 158 [[1803.09916](#)].
- [39] G. Bevilacqua, H. Hartanto, M. Kraus, T. Weber and M. Worek, *Towards constraining Dark Matter at the LHC: Higher order QCD predictions for $t\bar{t} + Z(Z \rightarrow \nu_\ell \bar{\nu}_\ell)$* , *JHEP* **11** (2019) 001 [[1907.09359](#)].
- [40] A. Denner, J.-N. Lang and M. Pellen, *Full NLO QCD corrections to off-shell ttbb production*, [2008.00918](#).
- [41] G. Bevilacqua, M. Czakon, M. Garzelli, A. van Hameren, A. Kardos, C. Papadopoulos et al., *HELAC-NLO*, *Comput. Phys. Commun.* **184** (2013) 986 [[1110.1499](#)].
- [42] A. van Hameren, C. Papadopoulos and R. Pittau, *Automated one-loop calculations: A Proof of concept*, *JHEP* **09** (2009) 106 [[0903.4665](#)].
- [43] G. Ossola, C. G. Papadopoulos and R. Pittau, *CutTools: A Program implementing the OPP reduction method to compute one-loop amplitudes*, *JHEP* **03** (2008) 042 [[0711.3596](#)].
- [44] M. Czakon, C. Papadopoulos and M. Worek, *Polarizing the Dipoles*, *JHEP* **08** (2009) 085 [[0905.0883](#)].
- [45] G. Bevilacqua, M. Czakon, M. Kubocz and M. Worek, *Complete Nagy-Soper subtraction for next-to-leading order calculations in QCD*, *JHEP* **10** (2013) 204 [[1308.5605](#)].
- [46] A. van Hameren, *Kaleu: A General-Purpose Parton-Level Phase Space Generator*, [1003.4953](#).

- [47] J. Butterworth et al., *PDF4LHC recommendations for LHC Run II*, *J. Phys. G* **43** (2016) 023001 [[1510.03865](#)].
- [48] NNPDF collaboration, *Parton distributions for the LHC Run II*, *JHEP* **04** (2015) 040 [[1410.8849](#)].
- [49] A. Buckley, J. Ferrando, S. Lloyd, K. Nordstrom, B. Page, M. Ruefenacht et al., *LHAPDF6: parton density access in the LHC precision era*, *Eur. Phys. J. C* **75** (2015) 132 [[1412.7420](#)].
- [50] M. Cacciari, G. P. Salam and G. Soyez, *The anti- k_t jet clustering algorithm*, *JHEP* **04** (2008) 063 [[0802.1189](#)].
- [51] D. Krohn, M. D. Schwartz, T. Lin and W. J. Waalewijn, *Jet Charge at the LHC*, *Phys. Rev. Lett.* **110** (2013) 212001 [[1209.2421](#)].
- [52] W. J. Waalewijn, *Calculating the Charge of a Jet*, *Phys. Rev. D* **86** (2012) 094030 [[1209.3019](#)].
- [53] ATLAS AND CMS collaboration, *Jet charge determination at the LHC*, [ATL-PHYS-PROC-2017-017](#) (2017) .
- [54] ATLAS collaboration, *Measurement of the Jet Vertex Charge algorithm performance for identified b -jets in $t\bar{t}$ events in pp collisions with the ATLAS detector*, [ATLAS-CONF-2018-022](#) (2018) .
- [55] F. C. Porter, *Testing Consistency of Two Histograms*, [0804.0380](#).
- [56] W. Bernreuther and Z.-G. Si, *Top quark and leptonic charge asymmetries for the Tevatron and LHC*, *Phys. Rev. D* **86** (2012) 034026 [[1205.6580](#)].
- [57] M. Czakon, D. Heymes, A. Mitov, D. Pagani, I. Tsinikos and M. Zaro, *Top-quark charge asymmetry at the LHC and Tevatron through NNLO QCD and NLO EW*, *Phys. Rev. D* **98** (2018) 014003 [[1711.03945](#)].
- [58] G. Bevilacqua, H. Hartanto, M. Kraus, T. Weber and M. Worek, *Off-shell vs on-shell modelling of top quarks in photon associated production*, *JHEP* **03** (2020) 154 [[1912.09999](#)].
- [59] M. Czakon, P. Fiedler and A. Mitov, *Resolving the Tevatron Top Quark Forward-Backward Asymmetry Puzzle: Fully Differential Next-to-Next-to-Leading-Order Calculation*, *Phys. Rev. Lett.* **115** (2015) 052001 [[1411.3007](#)].
- [60] M. Czakon, P. Fiedler, D. Heymes and A. Mitov, *NNLO QCD predictions for fully-differential top-quark pair production at the Tevatron*, *JHEP* **05** (2016) 034 [[1601.05375](#)].
- [61] CMS collaboration, *Measurement of the charge asymmetry in top-quark pair production in proton-proton collisions at $\sqrt{s} = 7$ TeV*, *Phys. Lett. B* **709** (2012) 28 [[1112.5100](#)].
- [62] ATLAS collaboration, *Measurement of the charge asymmetry in top quark pair production in pp collisions at $\sqrt{s} = 7$ TeV using the ATLAS detector*, *Eur. Phys. J. C* **72** (2012) 2039 [[1203.4211](#)].
- [63] CMS collaboration, *Measurements of $t\bar{t}$ charge asymmetry using dilepton final states in pp collisions at $\sqrt{s} = 8$ TeV*, *Phys. Lett. B* **760** (2016) 365 [[1603.06221](#)].
- [64] ATLAS collaboration, *Measurements of the charge asymmetry in top-quark pair production in the dilepton final state at $\sqrt{s} = 8$ TeV with the ATLAS detector*, *Phys. Rev. D* **94** (2016) 032006 [[1604.05538](#)].

- [65] ATLAS, CMS collaboration, *Combination of inclusive and differential $t\bar{t}$ charge asymmetry measurements using ATLAS and CMS data at $\sqrt{s} = 7$ and 8 TeV*, *JHEP* **04** (2018) 033 [[1709.05327](#)].
- [66] ATLAS COLLABORATION collaboration, *Inclusive and differential measurement of the charge asymmetry in $t\bar{t}$ events at 13 TeV with the ATLAS detector*, Tech. Rep. ATLAS-CONF-2019-026, CERN, Geneva, Jul, 2019.
- [67] CMS collaboration, *Inclusive and differential measurements of the $t\bar{t}$ charge asymmetry in pp collisions at $\sqrt{s} = 8$ TeV*, *Phys. Lett. B* **757** (2016) 154 [[1507.03119](#)].
- [68] S. Jung, A. Pierce and J. D. Wells, *Top quark asymmetry from a non-Abelian horizontal symmetry*, *Phys. Rev. D* **83** (2011) 114039 [[1103.4835](#)].
- [69] P. Ferrario and G. Rodrigo, *Massive color-octet bosons and the charge asymmetries of top quarks at hadron colliders*, *Phys. Rev. D* **78** (2008) 094018 [[0809.3354](#)].
- [70] J. Aguilar-Saavedra and M. Perez-Victoria, *Asymmetries in $t\bar{t}$ production: LHC versus Tevatron*, *Phys. Rev. D* **84** (2011) 115013 [[1105.4606](#)].
- [71] E. Alvarez, A. Juste, M. Szewc and T. Vazquez Schroeder, *Topping-up multilepton plus b -jets anomalies at the LHC with a Z' boson*, [2011.06514](#).
- [72] J. Aguilar-Saavedra and M. Perez-Victoria, *Shaping the top asymmetry*, *Phys. Lett. B* **705** (2011) 228 [[1107.2120](#)].